J. Micropalaeontology, 43, 211–238, 2024
https://doi.org/10.5194/jm-43-211-2024


Journal of Micropalaeontology
Open Access

# Pliocene–Pleistocene warm-water incursions and water mass changes on the Ross Sea continental shelf (Antarctica) based on foraminifera from IODP Expedition 374

**Julia L. Seidenstein[1,2], R. Mark Leckie[2], Robert McKay[3], Laura De Santis[4], David Harwood[5], and IODP Expedition 374 Scientists✚**

[1]U.S. Geological Survey, Florence Bascom Geoscience Center, 12201 Sunrise Valley Dr MS926A, Reston, VA 20192, USA
[2]Department of Earth, Geographic, and Climate Sciences, University of Massachusetts Amherst, Amherst, MA 01003, USA
[3]Antarctic Research Centre, Victoria University of Wellington, Wellington, New Zealand
[4]National Institute of Oceanography and Applied Geophysics – OGS, Trieste, Italy
[5]Department of Earth and Atmospheric Sciences, University of Nebraska-Lincoln, Lincoln, NE 68588, USA
✚A full list of authors and their affiliations appears at the end of the paper.

**Correspondence:** Julia L. Seidenstein (jseidenstein@usgs.gov)

Received: 30 June 2023 – Revised: 12 April 2024 – Accepted: 6 May 2024 – Published: 11 July 2024

**Abstract.** International Ocean Discovery Program (IODP) Expedition 374 sailed to the Ross Sea in 2018 to reconstruct paleoenvironments, track the history of key water masses, and assess model simulations that show warm-water incursions from the Southern Ocean led to the loss of marine-based Antarctic ice sheets during past interglacials. IODP Site U1523 (water depth 828 m) is located at the continental shelf break, northeast of Pennell Bank on the southeastern flank of Iselin Bank, where it lies beneath the Antarctic Slope Current (ASC). This site is sensitive to warm-water incursions from the Ross Sea Gyre and modified Circumpolar Deep Water (mCDW) today and during times of past warming climate. Multiple incursions of subpolar or temperate planktic foraminifera taxa occurred at Site U1523 after 3.8 Ma and prior to ∼1.82 Ma. Many of these warm-water taxa incursions likely represent interglacials of the latest Early Pliocene and Early Pleistocene, including Marine Isotope Stage (MIS) Gi7 to Gi3 (∼3.72–3.65 Ma), and Early Pleistocene MIS 91 or 90 (∼2.34–2.32 Ma) and MIS 77–67 (∼2.03–1.83 Ma) and suggest warmer-than-present conditions and less ice cover in the Ross Sea. However, a moderately resolved age model based on four key events prohibits us from precisely correlating with Marine Isotope Stages established by the LR04 Stack; therefore, these correlations are best estimates. Diatom-rich intervals during the latest Pliocene at Site U1523 include evidence of anomalously warm conditions based on the presence of subtropical and temperate planktic foraminiferal species in what likely correlates with interglacial MIS G17 (∼2.95 Ma), and a second interval that likely correlates with MIS KM3 (∼3.16 Ma) of the mid-Piacenzian Warm Period. Collectively, these multiple incursions of warmer-water planktic foraminifera provide evidence for polar amplification during super-interglacials of the Pliocene and Early Pleistocene. Higher abundances of planktic and benthic foraminifera during the Mid- to Late Pleistocene associated with interglacials of the MIS 37–31 interval (∼1.23–1.07 Ma), MIS 25 (∼0.95 Ma), MIS 15 (∼0.60 Ma), and MIS 6–5e transition (∼0.133–0.126 Ma) also indicate a reduced ice shelf and relatively warm conditions, including multiple warmer interglacials during the Mid-Pleistocene Transition (MPT). A decrease in sedimentation rate after ∼1.78 Ma is followed by a major change in benthic foraminiferal biofacies marked by a decrease in *Globocassidulina subglobosa* and a decrease in mud (< 63 µm) after ∼1.5 Ma. Subsequent dominance of *Trifarina earlandi* biofacies beginning during MIS 15 (∼600 ka) indicate progressive strengthening of the Antarctic Slope Current along the

shelf edge of the Ross Sea during the mid to Late Pleistocene. A sharp increase in foraminiferal fragmentation after the MPT (~ 900 ka) and variable abundances of *T. earlandi* indicate higher productivity, a stronger but variable ASC during interglacials, and/or corrosive waters, suggesting changes in water masses entering (mCDW) and exiting (High Salinity Shelf Water or Dense Shelf Water) the Ross Sea since the MPT.

## 1 Introduction

### 1.1 Background

The West Antarctic Ice Sheet (WAIS) is predominantly grounded far below sea level and overlies a reverse slope bed and is therefore highly susceptible to marine ice sheet instability and collapse (Pritchard et al., 2012). If the WAIS collapses, the melting ice would cause a global sea level increase of ~ 3.5–5.0 m (Lythe et al., 2001; Pollard and DeConto, 2009; Bamber et al., 2009; DeConto and Pollard, 2016). During the Late Pliocene (~ 3.2–2.7 Ma), including the mid-Piacenzian Warm Period (mPWP; Dowsett et al., 2011; Raymo et al., 2011), with atmospheric carbon dioxide ($CO_2$) concentrations similar to today (330–415 ppm; Pagani et al., 2010), global sea level was $22 \pm 10$ m above present suggesting a complete collapse of both the Greenland Ice Sheet and the WAIS, as well as significant ice removal from the East Antarctic Ice Sheet (Miller et al., 2012; Grant et al., 2019). Scherer et al. (1998) speculated that a partial WAIS collapse occurred during the last 1 Myr, possibly during Marine Isotope Stage (MIS) 5e (~ 123 ka) or MIS 11 (~ 374–424 ka). WAIS collapse during past warm periods may be connected to an intensification of ocean–cryosphere interactions (Naish et al., 2009; Pollard and DeConto, 2009). Today, upwelling of Circumpolar Deep Water (CDW) is causing basal ice sheet melt and ice shelf thinning in the Bellingshausen and Amundsen sea sectors of the WAIS margin (Dinniman et al., 2011; Pritchard et al., 2012; Majewski, 2013; Jenkins et al., 2016; Hillenbrand et al., 2017). Changes in the circulation of Antarctic Surface Water (AASW) and in Antarctic Bottom Water (AABW) production or changes in the wind-driven Antarctic Slope Current (ASC) strength and position control the incursion of CDW onto the shelf break and flooding of the Ross Sea shelf, thus leading to melting and retreat of the Ross Ice Shelf (Thompson et al., 2018) (Fig. 1). The CDW is relatively warm (> 0 °C), saline (> 34.6 ‰), and nutrient-rich compared to the shelf waters in the Ross Sea (Castagno et al., 2017; Morrison et al., 2020; Wang et al., 2023). In the Ross Sea, CDW becomes modified CDW (mCDW) by mixing with AASW, High Salinity Shelf Water (HSSW), and/or Ice Shelf Water (ISW). The mCDW then affects the Ross Sea Polynya and the formation of Ross Sea Bottom Water (RSBW), which feeds AABW, as well as supplying the heat that is transported beneath the Ross Ice Shelf and contributes to basal melting (Orsi and Wiederwohl, 2009).

The eastward-flowing Antarctic Circumpolar Current (ACC), driven by strong westerly winds, has been shown to flow faster and stronger during deglaciation and warmer-than-present interglacials of the Pliocene–Pleistocene (Bostock et al., 2013; Wu et al., 2021; Lamy et al., 2024). The Antarctic Slope Current (ASC) is the southern limb of the Ross Gyre, an eddy of the ACC, that flows strongly westward as a contour current along the upper continental margin of the Ross Sea, driven in part by the Polar easterlies (Smith et al., 2012; Thompson et al., 2018; Kim et al., 2020). The Antarctic Slope Front defines the southern boundary of the ASC, which is a barrier between Antarctic Surface Water (AASW) and Circumpolar Deep Water (CDW) impinging on the continental margin (Jacobs, 1991; Orsi and Wiederwohl, 2009; Si et al., 2023). If the Antarctic Slope Front is shallow, CDW can enter the continental shelf, mix with shelf waters, and become mCDW (Whitworth and Orsi, 2006; Orsi and Whitworth, 2009; Budillon et al., 2011; Dinniman et al., 2011; Pardo et al., 2012; Castagno et al., 2017). Tidal mixing is also important in the creation of mCDW near the shelf edge (Castagno et al., 2017; Si et al., 2023), as well as the bathymetry (Gales et al., 2021). Si et al. (2023) demonstrate that freshening of shelf waters due to increased melting leads to increased shoreward heat flux, which is a positive feedback during times of warmer climate. Upwelling and mixing of CDW with surface waters along the Antarctic Slope Front also introduces a significant source of dissolved iron for primary productivity (Dinniman et al., 2011; Smith et al., 2012).

Dense Shelf Water (DSW), High Salinity Shelf Water (HSSW), Ice Shelf Water (ISW), or Ross Sea Bottom Water (RSBW) are exported off the continental shelf along the lower western slopes of the deeper troughs (e.g., Drygalski, Joides, Glomar Challenger), while AASW and CDW are imported onto the shelf on the eastern mid to upper slopes of the troughs (Budillon et al., 2011; Dinniman et al., 2011; Castagno et al., 2017; Colleoni et al., 2018; Kim et al., 2020; Morrison et al., 2020; Conte et al., 2021; Bollen et al., 2022). Morrison et al. (2020) used a global, eddying ocean model to show that warm CDW transport onto the Antarctic shelf is driven by local DSW export in canyons. Dinniman et al. (2011) suggest that CDW and mCDW intrusions are at least partially related to short-duration wind events. Castagno et al. (2017) documented seasonal variability in CDW incursions onto the shelf with strong inflow early in the austral summer (late December/early January). Like the ACC, the ASC may have been stronger and flowed faster during deglacial and interglacial times, which winnowed sedi-

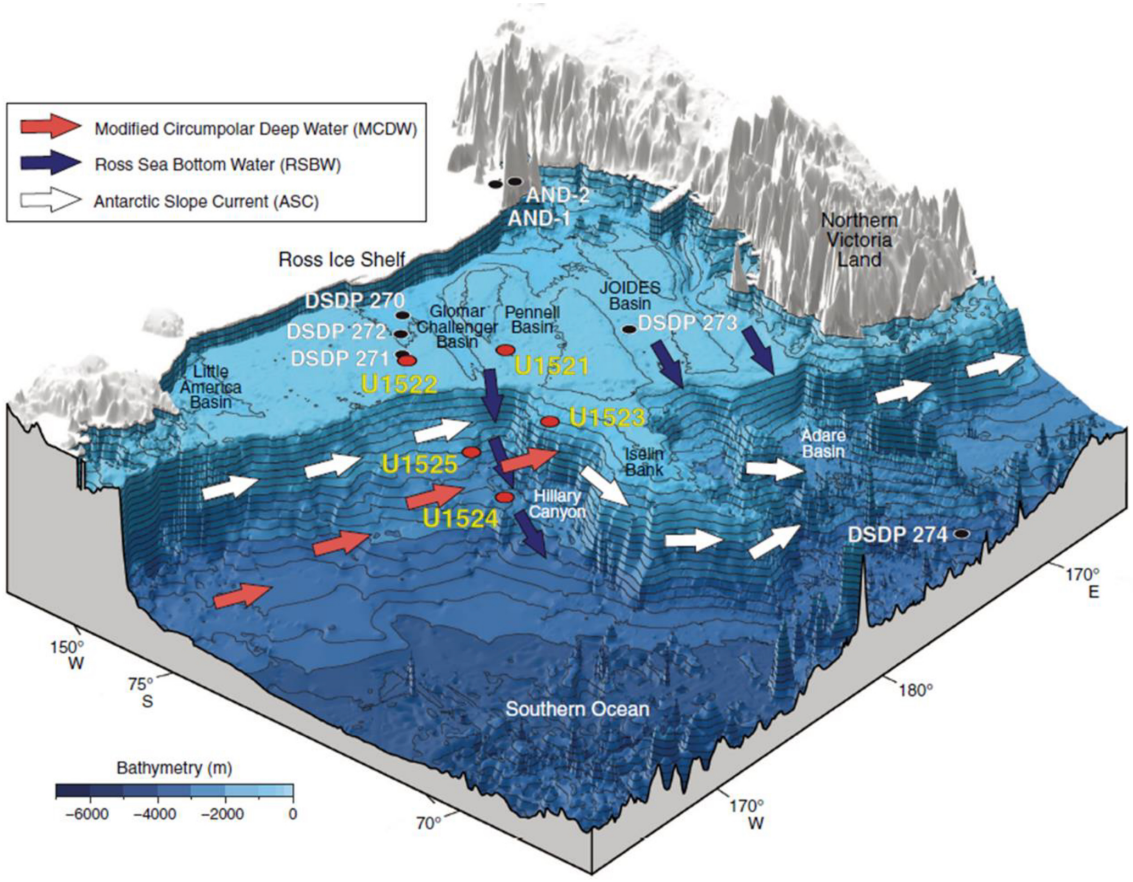


**Figure 1.** Bathymetric diagram showing the locations of IODP Expedition 374 Sites U1521–U1525 (red circles), DSDP Leg 28 Sites 270–274 (black circles), and ANDRILL Cores AND-1B and AND-2A (black circles). Figure from McKay et al. (2019).

ments near the shelf edge of the northwestern Iselin Bank, creating clast-rich muddy sands with planktic and benthic foraminifera, and increased export of Dense Shelf Water and incursions of CDW and mCDW (Bollen et al., 2022). However, other studies have interpreted glacials as associated with stronger ASC flow near the shelf edge (Conte et al., 2021), with clast- and planktic-foraminifer-rich, diatom-poor muddy sand on the Iselin Bank (e.g., Kim et al., 2020). The position and strength of the polar easterlies, varying across different timescales including glacial–interglacial cycles, drives ASC strength and its effectiveness in allowing the incursions of CDW and mCDW onto the Ross Sea continental shelf (Thompson et al., 2018; Conte et al., 2021; Bollen et al., 2022). Processes on the continental shelf involved with the formation and ultimate export of dense waters off the shelf also control the incursion of CDW and mCDW onto the shelf (e.g., Pardo et al., 2012; Morrison et al., 2020; Bollen et al., 2022).

IODP Site U1523 lies beneath the modern-day westward-flowing Antarctic Slope Current (ASC) on the shelf break, northeast of Pennell Bank on the southeastern flank of Iselin Bank, in 828 m of water (Fig. 1). The ASC influences the southward incursions of mCDW onto the Ross Sea continental shelf (Kim et al., 2020; Morrison et al., 2020; Conte et al., 2021; Gales et al., 2021; Bollen, et al., 2022). One of the primary objectives of coring at Site U1523 was to reconstruct the vigor of the ASC during the Pliocene–Pleistocene and test the relationship between ASC current velocity and incursions of mCDW (McKay et al., 2019). In this study, we examine benthic foraminiferal biofacies that are indicative of ASC flow and/or mCDW incursion and thus an indicator of less sea ice or a smaller WAIS. A second major objective of coring at Site U1523 was to test for evidence of polar amplification during Pliocene–Pleistocene interglacials (McKay et al., 2019). The discovery of sporadic incursions of warmer-water planktic foraminifera allows us to address this issue. Lastly, the generation of moderately resolved foraminiferal records allows us to correlate this outer-shelf site with other DSDP and IODP shelf sites and ANDRILL-1B to assess the relationship between periods of glacial advance and retreat and changing water masses and productivity near the continental shelf break.

### 1.2 Foraminifera in the Ross Sea

The distribution of planktic foraminifera around Antarctica is controlled by the Antarctic Polar Front, the transition zone between Subantarctic Surface Water (SASW) and Antarctic Surface Water (AASW), and the Subantarctic Front, which is the zone between the Polar Front and the rest of the Southern Ocean to the north (Nelson and Cook, 2001; Sokolov and Rintoul, 2009; Freeman et al., 2016; Sangiorgi et al., 2018). Malinverno et al. (2016) conducted a latitudinal transect of all extant fossilizable planktonic groups from surface waters of the western Pacific sector of the Southern Ocean, from ∼ 48° S offshore New Zealand to ∼ 70° S in the Ross Sea. They reported that peak values of heterotrophic micro-zooplankton, including the dinoflagellate genus *Protoperidinium*, planktic foraminifera, and the tintinnid species *Codonellopsis pusilla*, occur in the Polar Frontal Zone, between the Southern Subantarctic Front (SSAF; ∼ 58.5° S, ∼ 5 °C) to the north and the Polar Front (PF; ∼ 62.8° S, ∼ 3 °C). This zone is also characterized by a monospecific assemblage of the coccolithophorid species *Emiliania huxleyi*, and a nearly monospecific assemblage of the silicoflagellate *Stephanocha* (formerly *Distephanus*) *speculum*. The diatom assemblage includes the persistence of taxa with subtropical affinities and an increase in cold, open-ocean taxa, including *Fragilariopsis kerguelensis*, the principal contributor to the Southern Ocean diatom ooze belt. Climatically driven changes in planktic foraminiferal distribution could indicate fluctuations in the latitudinal distribution of these water mass fronts due to increased warming, weakening of the Antarctic Circumpolar Current (ACC), changes in sea ice cover, and ocean productivity.

Benthic foraminifera are proxies of past environmental conditions on the seafloor and provide information about the characteristics of bottom water masses (e.g., carbonate chemistry), bottom water currents, sea ice cover, productivity, sub-ice-shelf conditions, and proximity to the grounding zone. Numerous studies have investigated modern, Quaternary, and Neogene foraminiferal assemblages and their environments in the Ross Sea and around the Antarctic continental margin (e.g., McKnight, 1962; Kennett, 1966, 1968; Pflum, 1966; Fillon, 1974; Kellogg et al., 1979; Osterman and Kellogg, 1979; Leckie and Webb, 1983, 1986; Ward and Webb, 1986; Ward et al., 1987; Ishman and Webb, 1988; Webb and Strong, 2000; Ishman and Szymcek, 2003; Szymcek et al., 2007; Melis and Salvi, 2009; Patterson and Ishman, 2012; Majewski et al., 2016, 2018, 2020; Prothro et al., 2018; Melis and Salvi, 2020; Melis et al., 2021). Deglacial sediments beneath the Ross Ice Shelf and proximal to retreating grounding zone wedges typically preserve calcareous benthic and planktic foraminifera. Calcareous foraminifera are also better preserved in coarser sediments that have been winnowed of organic-rich fines or biosiliceous muds (e.g., Prothro et al., 2018). By contrast, interglacial open-shelf sediments are often characterized by agglutinated benthics due to presence of corrosive biosiliceous muds or where exposed to corrosive High Salinity Shelf Water. The carbonate compensation depth (CCD) is relatively shallow in the Ross Sea (∼ 400–700 m) and elsewhere around the continental margin and is therefore also a factor on foraminiferal distribution and preservation (Kennett, 1966, 1968; Anderson, 1975; Osterman and Kellogg, 1979; Milam and Anderson, 1981; Melis and Salvi, 2009; Majewski, 2013). The Ross Sea contains five north–south-trending troughs with depths exceeding 900 m in places, and the shallow CCD changes with the bathymetry (Osterman and Kellogg, 1979).

### 1.3 Climatic events in the Ross Sea

Based on the ANDRILL-1B (AND-1B) core from the McMurdo Sound area, there was a smaller WAIS and reduced sea ice extent before 3.3 Ma, followed by Southern Ocean cooling and seasonal expansion of sea ice from 3.3 to 2.6 Ma (McKay et al., 2012a). This Southern Ocean cooling strengthened winds and ocean circulation, which led to a reduced Atlantic Meridional Overturning Circulation (AMOC) and helped facilitate the conditions for Northern Hemisphere glaciation (McKay et al., 2012a). Patterson et al. (2014) proposed that Southern Ocean cooling from 3.5 to 2.5 Ma restricted the upwelling of warm $CO_2$-rich CDW at the margins of Antarctica. As a result, the melt season was restricted to times of austral summer insolation maxima controlled by precession. This decrease in radiative forcing caused extensive sea ice cover that extended into the summer season and limited the influence of upwelling CDW onto the continental shelf, and consequently the influence of this water mass in triggering enhanced ice sheet melt was reduced (Patterson et al., 2014).

The Mid-Pleistocene Transition (MPT) occurred from ∼ 1.25 to 0.75 Ma (Herbert, 2023). Elderfield et al. (2012) suggested that the MPT could have begun during MIS 23, as the Antarctic ice that formed in MIS 24 was not fully melted, leading to ice growth and a large Antarctic ice sheet during MIS 22. This evidence suggests that the MPT was controlled by the growth and increased stability of Antarctic ice volume since ∼ 0.9 Ma. Marine Isotope Stage 31 (1.08–1.06 Ma) is considered a "super-interglacial" event within the MPT (Scherer et al., 2008; Pollard and DeConto, 2009; DeConto et al., 2012; McKay et al., 2012b; Melles et al., 2012). MIS 31 is a likely interglacial with good evidence for significantly reduced sea ice and ice shelf in the Ross Sea, possibly leading to the collapse of the WAIS (Naish et al., 2009; McKay et al., 2012a). Climate modeling predicts an almost complete collapse of the WAIS during MIS 31, with sub-ice-shelf ocean melting as the driver of this collapse, while surface ice melting was insignificant (DeConto et al., 2012; Beltran et al., 2020). Following MIS 31, MIS 5e and 11 are additional possible warming events that have been investigated for marine-based Antarctic ice sheet collapse or partial collapse (Scherer et al., 1998; Hearty et al., 2007; Overpeck

et al., 2006; Duplessy et al., 2007; Hillenbrand et al., 2009; Wilson et al., 2018).

## 2 Materials and methods

### 2.1 IODP Expedition 374 Site U1523

International Ocean Discovery Program (IODP) Expedition 374 cored five sites (Fig. 1) at a range of water depths on the Ross Sea shelf, slope, and rise from January to March 2018 using the *JOIDES Resolution* drilling vessel. This study focuses on the Pliocene–Pleistocene interval of Site U1523, located on the shelf break. A companion study focuses on the Pleistocene foraminifera of the slope (U1525) and rise (U1524) sites cored during Expedition 374 (Bombard et al., 2023). Site U1523 (74°0.02′ S, 179°47.70′ W) cored through a stratified sediment drift on the outermost continental shelf edge in water depth of 828 m (Fig. 1; McKay et al., 2019). We sampled three of the five holes drilled at Site U1523: Hole U1523A recovered 33.51 m of core (72 % recovery), Hole U1523B recovered 45.13 m (37 %), and Hole U1523E recovered 54.08 m (64 %) (Fig. 2). However, this is misleading for the total recovery of the stratigraphy at this site, with a total of 91 m of the stratigraphy recovered down to 130 m b.s.f. (70 % recovery), while drilling parameters and downhole log data indicate most of the missing recovery was due to the presence of coarse gravel lags (McKay et al., 2019). Consequently, a composite section was developed using detailed stratigraphic descriptions and XRF analysis (Kulhanek et al., 2022). Three lithologic units are recognized in the composite Site U1523 section. This study focused on Unit I and Unit II; an unconformity separates Unit II and Unit III. Unit I comprises ∼ 34.7–36.9 m of massive, bioturbated to laminated, greenish gray to grayish brown diatom-bearing to diatom-rich mud, interbedded at the decimeter scale with diatom-bearing and foraminifer-bearing muddy sand and diamict with dispersed clasts. Unit II comprises ∼ 61 m of massive, bioturbated to laminated greenish gray diatom-bearing to diatom-rich mud and olive brown to gray diatom-rich mud to muddy diatom ooze, interbedded at the decimeter to meter scale with massive bioturbated gray to greenish gray diamict (McKay et al., 2019; Gales et al., 2023). Unit II is more diatomaceous than Unit I and it contains discrete beds of diatom ooze. Based on the age model used in this study, Unit I is Early Pleistocene (∼ 2.2 Ma, MIS 84 or 85) to Holocene in age, while Unit II is late Early Pliocene to Early Pleistocene in age (∼ 3.8–2.2 Ma).

Site U1523 is located on the northeastern edge of Pennell Bank, above Hillary Canyon (Fig. 1; McKay et al., 2019; Gales et al., 2023). This location was chosen because it lies beneath the westward-flowing Antarctic Slope Current (ASC; Orsi and Widerwohl, 2009). Sediment at this site was derived from multiple sources, including icebergs from the east via the Ross Sea Gyre and ASC, downslope delivery by glacial outwash, or suspended sediment and pelagic and hemipelagic sedimentation (McKay et al., 2019; Gales et al., 2023). Seismostratigraphic and oceanographic data, in addition to modeling experiments, indicate winnowing of the fine-grained sediment at this site is likely during times of strong bottom-current flow associated with shifts in the wind-driven ASC (Jacobs et al., 1974; Conte et al., 2021).

### 2.2 Core samples and raw data

In August 2018, samples (20 $cm^3$) specifically for micropaleontology work were taken at the IODP Gulf Coast Core Repository as part of the post-expedition sampling party. The samples were taken about every 0.75 m and sometimes shifted by a few centimeter to accommodate other sampling. These 100 samples, along with 9 core catcher samples processed during the expedition, were the original focus from the 95 m Pliocene–Pleistocene section of Site U1523. An additional 22 samples were taken from U1523 in June 2019 to increase the sampling resolution around the Mid-Pleistocene Transition (MPT). A total of 131 samples from Site U1521 were examined for foraminifera in this study. Data of the raw foraminifera counts is published on the USGS ScienceBase online data repository located at https://www.sciencebase.gov/catalog/item/653914f0d34ee4b6e05bbb1e, last access: 28 June 2024.

### 2.3 Sample preparation and foraminiferal abundance

Samples were processed a few weeks after acquisition by freeze drying each sample, washing them through a 63 µm sieve, and drying overnight at 50 °C. Some samples were soaked for up to 12 h in DI water before washing because they were harder to disaggregate. Foraminifera, including planktic, calcareous benthic, and agglutinated tests were picked from the > 125 µm size fraction. To prepare for picking, each sample was dry sieved through 841 and 125 µm sieves to obtain the 125–841 µm fraction. Samples with a large amount of material were split using a microsplitter and then spread onto a microfossil picking tray. Planktic and benthic foraminifers were picked until a total of 300 whole specimens was reached, whenever possible. Since 300 specimens were rarely present, any assemblage with more than 10 specimens was included in the study. Of the 131 samples examined from Site U1523, 66 (50.4 %) have 10 or more specimens of benthic foraminifera (Fig. 6), while 64 (48.8 %) have 10 or more specimens of planktic foraminifera (Fig. 5). In addition, counts were made of both benthic and planktic fragments, though these were not picked. Total foraminifera are reported as number of foraminifera per gram of sediment (Fig. 4), but we acknowledge that the number of foraminifera per gram sediment can change through a change in the number of living foraminifers, a change in sedimentation processes, or both. Sedimentological weights were collected by weighing the freeze-dried sample before it was washed through the > 63 µm sieve and subtracting the washed and

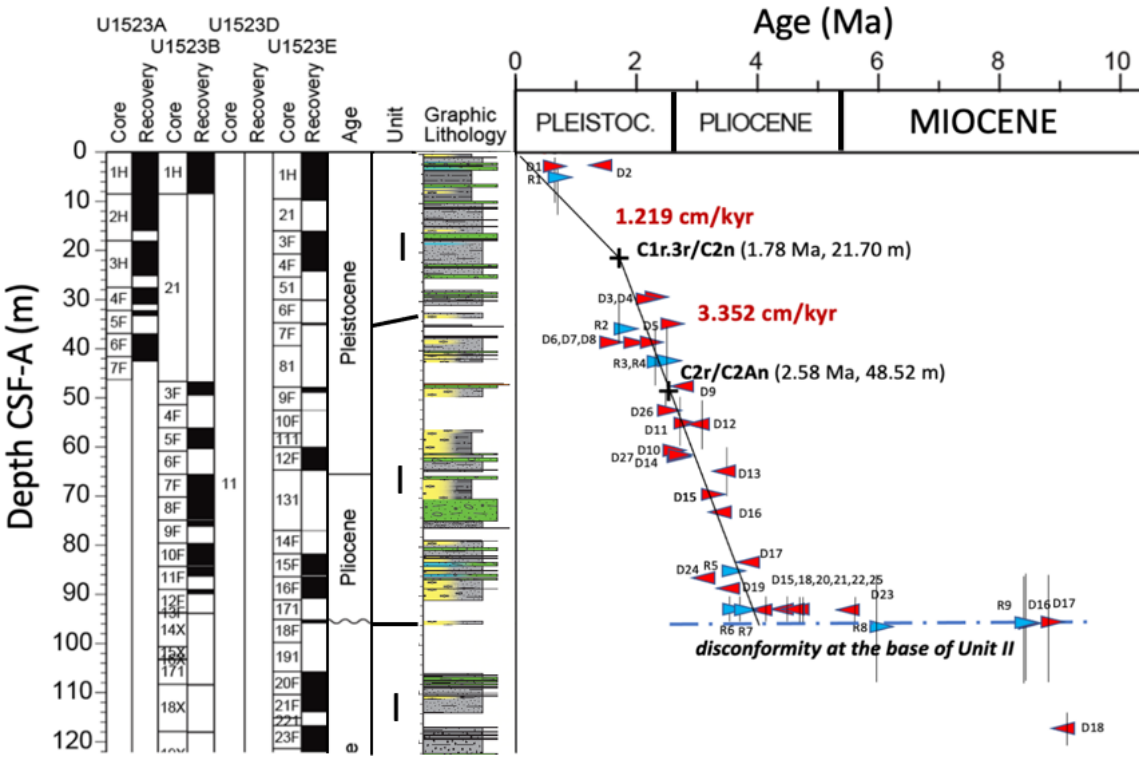


**Figure 2.** Age model for Site U1523 showing biochronologic events, paleomagnetic reversals, and unconformities. Vertical black bars show uncertainty caused by gaps between samples. Figure adapted from McKay et al. (2019) and Gales et al. (2023). Age model created from two magnetochron boundaries, C1r.3r/C2n (1.78 Ma) at 21.70 m and C2r/C2An (2.58 Ma) at 48.52 m, and supported by diatom (red triangles) and radiolarian (blue triangles) biostratigraphic datums. In addition to the two paleomagnetic reversals, two additional paleoclimatic events anchor the lower and upper ends of the age model: Marine Isotope Stage (MIS) Gi7 (3.72 Ma, LR04 stack) at 86.75 m GSF-B and MIS 5e (0.123 Ma, LR04 stack) at 1.54 m GSF-B. See text for details. Under "Graphic Lithology", blue indicates foraminifera-bearing samples, yellow indicates diatom-bearing or diatom-rich ooze, dotted gray indicates sandy mud or muddy sand, dashed gray indicates mud, and green indicates diamict samples (Gales et al., 2023).

dried weight from the original to get the silt and clay size fraction (< 63 µm). Following this, the sand fraction (63 µm to 2 mm) and gravel (> 2 mm) weights were measured for each sample (Fig. 4).

### 2.4 Q-mode and R-mode cluster analysis

A combined Q-mode and R-mode cluster analysis was performed on a subset of the benthic foraminifera data using the PAleo STatistics program (PAST 4.13; Hammer et al., 2001; Hammer, 2003) with the algorithm setting for paired group and similarity index for Bray–Curtis. The Bray–Curtis similarity index is based on relative abundance data, while the Jaccard index is based on presence–absence data, and the Euclidean distance index works best with samples that have continuous abundance data (e.g., Lagoe, 1979; Patterson and Ishman, 2012; Bombard et al., 2024). A rarefaction analysis (Sanders, 1968) allows comparison of samples with different sizes by considering the relationship between the number of species in a sample versus the number of specimens. The shape of the species abundance curve decreases at a logarithmic rate as the number of specimens in a sample increases arithmetically. This analysis of all U1523 samples reveals that the species abundance curve begins to flatten out with ∼ 40–50 benthic specimens (Fig. 3). Of the 131 samples examined, 42 (32 % of the investigated samples) contain at least 40 benthic specimens, and of these the average number of specimens per sample is 84; 12 samples have > 100 specimens, while 36 samples have 50 or more specimens. Cluster analysis was performed on these 42 samples containing 40 or more benthic foraminiferal specimens. Only species that have a relative abundance of > 2 % in any one sample were included. R-mode tests for relationships among variables, in this case it groups species together rather than samples, to define biofacies (e.g., Lagoe, 1979; Leckie and Olson, 2003). The benthic genera percentages (relative to total number of benthic specimens) of these 42 samples were used in the cluster analysis to produce a two-way heat map and benthic biofacies (Fig. 7). In defining the clusters, benthic genera that occurred with relative abundances > 20 % in a majority of the samples in the cluster are considered primary taxa. Any benthic genera occurrence between 5 %–20 % in at least half

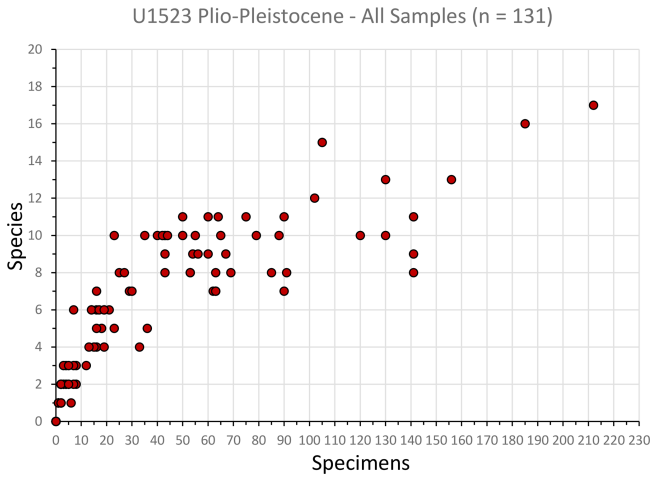


**Figure 3.** Rarefaction analysis (Sanders, 1968) of all 131 foraminiferal samples examined in this study. The number of species flattens out between 40 and 50 specimens. We used a cutoff of 40 specimens for samples to be included in the cluster analysis; a total of 42 samples (32 % of all samples) were included in the cluster analysis to identify benthic foraminiferal biofacies.

of the samples within a particular cluster are considered secondary or accessory taxa.

### 2.5 Chronostratigraphy and age model

The age model for U1523 covers much of the late Early Pliocene, Late Pliocene, and Pleistocene, from ∼ 3.83 Ma to present. The age model for this study, based on the shipboard work for Site U1523 and updated in Gales et al. (2023), was created using two magnetic reversals, C2r/C2An at 2.58 Ma (48.52 m) and C1r.3r/C2n at 1.78 Ma (21.7 m), and supported by numerous diatom and radiolarian biostratigraphic datums (McKay et al., 2019). Linear sedimentation rates are extrapolated from the lower magnetic reversal to the base of the study interval and from the upper magnetic reversal to the top of the core. Sedimentation rate decreases at 1.78 Ma from 3.352 to 1.219 cm $ky^{-1}$ (Fig. 2). While having only two control points through a 95 m section is not very satisfactory, the average sedimentation rates of the two segments below and above the magnetic reversal tie points yield very good correlations to well-known, well-dated paleoclimate events: the Marine Isotope Stage (MIS) Gi7–Gi3 interval (3.721–3.658 Ma) at 86.75–84.65 m and the Termination II–MIS 5e interval (0.133–0.126 Ma) at 1.63–1.54 m. This finding suggests that the age model is robust from top to bottom if we incorporate these two well-dated paleoclimatic events into the age model.

## 3 Results

### 3.1 Planktic and benthic foraminiferal occurrences

The U1523 samples reveal intervals of relatively high numbers of foraminifera alternating with few or none, as seen in the total planktics and benthics per sample, number of benthic species per sample, and the number of benthic and planktic foraminiferal specimens per gram of sediment (Fig. 4). The number of benthic species per sample is highest at 0–2, 12–20, and 22–29 m b.s.f. (0–0.1, 1–1.7, and 1.8–2.0 Ma, respectively). Foraminifera per gram of sediment for both planktics and benthics is highest at 1, 23–30, 40, and 84 m b.s.f. (0.1, 1.8–2.0, 2.3, and 3.6–3.7 Ma, respectively). Lithologic Unit II is significantly more diatomaceous than Unit I, and it has lower absolute abundances of planktic and benthic foraminifera (foraminifera per gram of sediment), particularly in the interval from ∼ 40–84 m b.s.f. (∼ 2.3 to 3.6 Ma; MIS 91 to MIS Gi3). Unit I also has reduced numbers of foraminifera in the interval from ∼ 1.6–13.2 m b.s.f. (∼ 0.26 to 1.08 MIS 5e to MIS 31). The percent fragments of benthics and planktics changes through the cored interval with fragmentation being low through much of the core except in the uppermost portions of the section where fragmentation is 25 %–50 % for benthics from 0–4 m b.s.f. (0–0.3 Ma), and 25 %–50 % for planktics from 0-10 m b.s.f. (0–0.9 Ma) (Fig. 4). For some intervals of the section, there are close to equal numbers of planktics and benthics, but there are consistently more planktics from 7–29 m b.s.f. (0.6–2.0 Ma) as seen by percent planktics > 50 %.

The percent abundance (by weight) of fine sediment changes through the study interval. In general, there is a decrease in percent mud (< 63 µm) above ∼ 14.5 m b.s.f. (1.5 Ma) (Fig. 4). Percent fines (silt and clay) are lower (< 50 % of the sample) around 10–18, 71, and 85 m b.s.f. (0.8–1.5, 3.3, 3.6–3.7 Ma, respectively). The clast-rich, sandy interval at ∼ 71–74 m b.s.f. likely correlates with the MIS M2 glacial event (∼ 3.31–3.26 Ma; Lisiecki and Raymo, 2005; McKay et al., 2012a, b), further supporting our age model.

Planktic foraminiferal assemblages (Fig. 5, Plate 1, Table 1) are dominated by polar *Neogloboquadrina pachyderma* throughout the Pliocene–Pleistocene of Site U1523. Subpolar *Neogloboquadrina incompta* is present through most of the section at abundances of < 10 %. Temperate *Globigerina bulloides* and *Globigerina falconensis* are very rare and occur ∼ 23–28, 40, and 85 m b.s.f. (∼ 1.8–2.0, 2.3, and 3.7 Ma, respectively). Subpolar *Turborotalita quinqueloba* is also very rare and is present ∼ 24 and 84–87 m b.s.f. (∼ 1.9 and 3.6–3.7 Ma). Tropical–subtropical *Globigerinoides ruber* (four tests) and temperate *Globoconella inflata* (six tests) occur in a single latest Pliocene sample at 59.5 m b.s.f. (∼ 2.95 Ma). *Globoconella inflata* is also recorded in a single sample from the Mid-Pleistocene at slope Site U1525 (Bombard et al., 2023). It is possible that these rare Ross Sea occur-

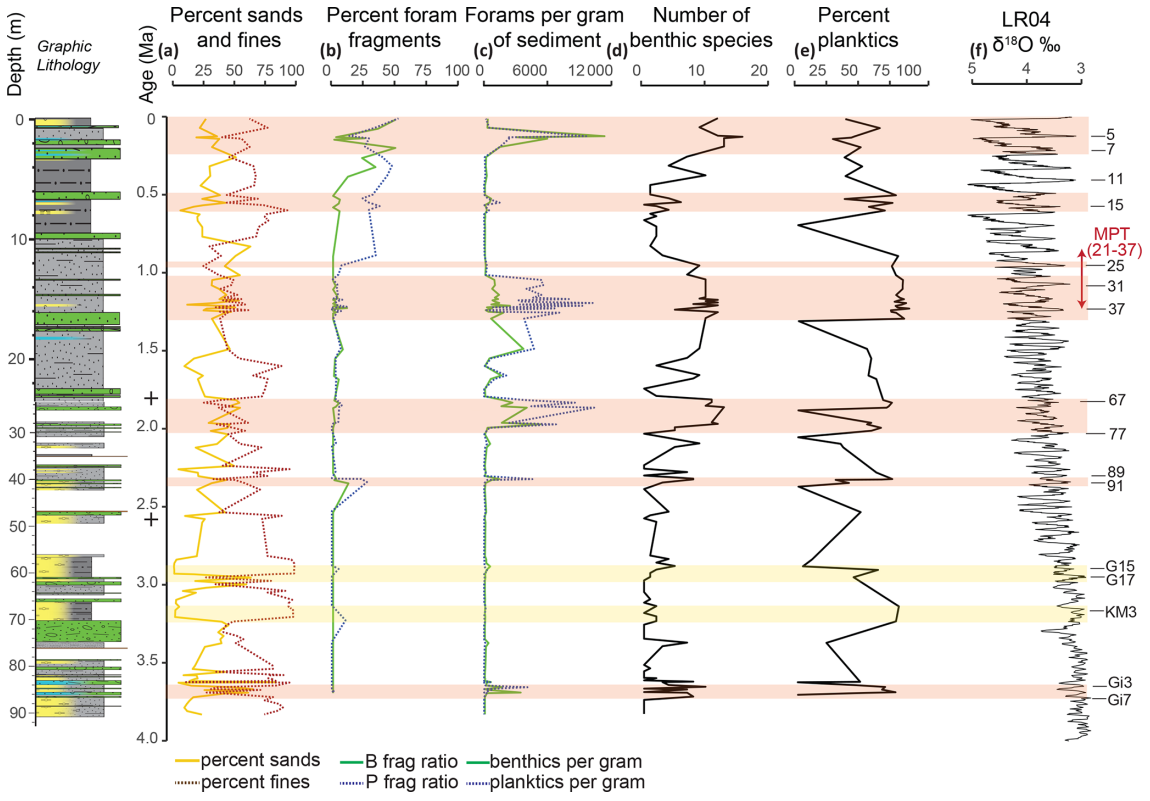


**Figure 4.** Sediment and foraminifera data from Site U1523 plotted against age (Ma). **(a)** Percent abundance of fines (dotted brown) and sand (yellow) in each sample based on weight. **(b)** Percent benthic foraminifera fragments (solid green) and planktic foraminifera fragments (dashed blue) represented in each sample relative to whole specimens. **(c)** Benthic foraminifers per gram of sediment (solid green), and planktic foraminifers per gram of sediment (dashed blue). **(d)** Simple diversity of number of benthic foraminifera species that occur in each sample. **(e)** Percent of total foraminifera picked that are planktic. **(f)** Benthic $\delta^{18}O$ stack of globally distributed benthic records (Lisiecki and Raymo, 2005) plotted against age with key interglacials listed on the right. Orange bars represent intervals with abundant foraminifera, corresponding closely with interglacials. Yellow bars represent weak layers 1 and 1b in diatom ooze (Gales et al., 2023). Next to the age scale are the two age points from magnetochron reversal boundaries represented by black crosses (Fig. 2). The graphic lithology is from Gales et al. (2023).

rences of *G. inflata* may represent the Type II subpolar genotype, in part based on their reduced apertural size (Morard et al., 2011). The total number of planktics varies through the section at Site U1523, with some samples being too small to include in the planktic abundance data; 64 samples (∼ 49 %) have 10 or more specimens of planktic foraminifera. The numbers of planktics are especially high (> 200 specimens) ∼ 13–16, 23–25, 40, and 85 m b.s.f. (∼ 1.1–1.3, 1.8–1.9, 2.3, and 3.6–3.7 Ma, respectively).

Benthic foraminiferal assemblages (Fig. 6, Plates 2–3, Table 1) are dominated by *Trifarina earlandi* and *Globocassidulina subglobosa*. Accessory taxa include, *Nonionella iridea*, *Rosalina globularis, Alabaminella weddellensis, Ehrenbergina glabra, Astrononion antarcticus, A. echolsi, Cibicides lobatulus, Globocassidulina biora*, and *Epistominella vitrea*. These taxa are all well known from the Antarctic continental shelf and upper slope (Pflum, 1966; Kennett, 1968; Fillon, 1974; Anderson, 1975; Osterman and Kellogg, 1979; Milam and Anderson, 1981; Ward and Webb, 1986, Ward et al., 1987; Ishman and Domack, 1994; Mellis and Salvi, 2009, 2020; Majewski, 2005, 2013; Majewski et al., 2016, 2018, 2020; Capotondi et al., 2018; Prothro et al., 2018; Melis et al., 2021). A total of 66 samples (∼ 50 %) have at least 10 specimens of benthic foraminifera; these 66 samples are shown on the data plots (Fig. 6).

### 3.2 Warm-water planktic foraminiferal occurrences and the U1523 age model

Compilation of planktic and benthic foraminifera occurrences at Site U1523 (Table 1) and a comparison of sample ages derived from our age model and the ages of the Marine Isotope Stages (MIS) derived from the Pliocene–Pleistocene benthic isotope stack (LR04; Lisiecki and Raymo, 2005) reveal very close correspondence between foraminiferal abundances and key paleoclimate events. For example, the MIS Gi7–Gi3 interval in the latest Early Pliocene is a widespread warming event in the Southern Ocean (Bohaty and Har-

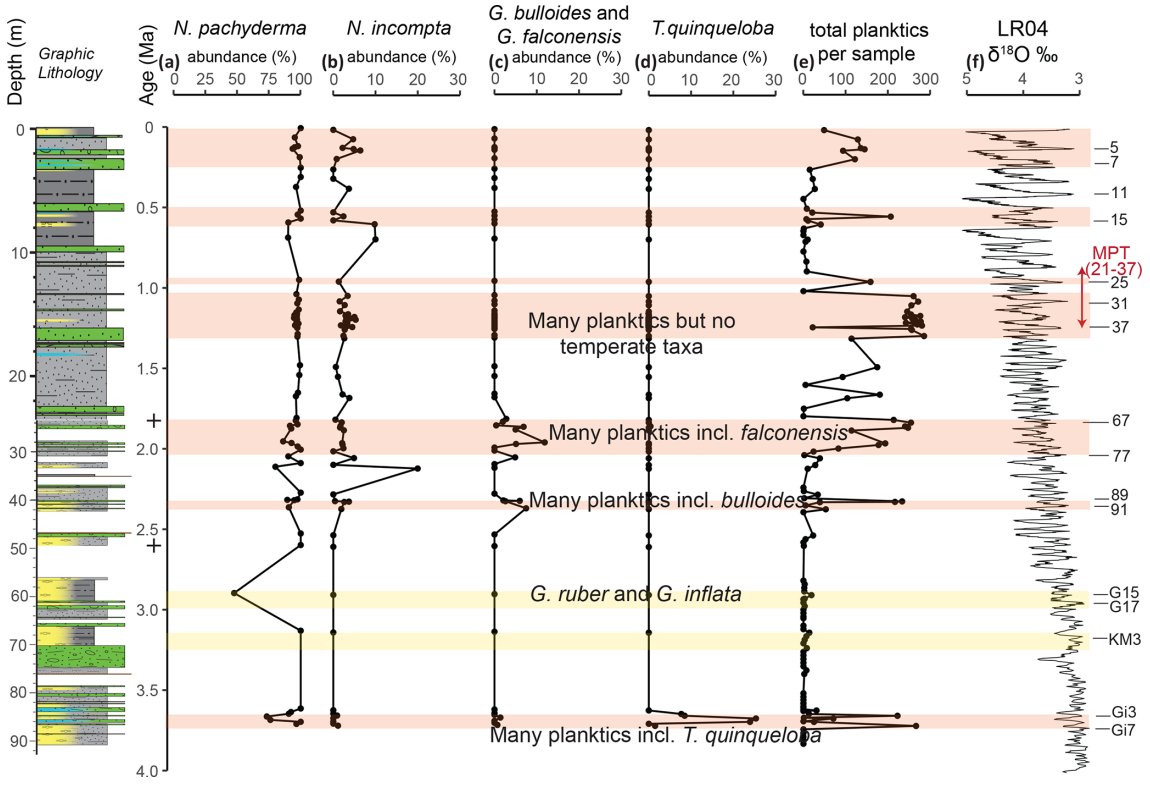


**Figure 5.** Relative abundance (%) of the major planktic foraminiferal species in U1523 plotted against age (Ma). Relative abundances for **(a)**–**(d)** were only plotted if there were more than 10 specimens in the sample ($n = 64$); all other samples were excluded. **(a)** *N. pachyderma* is the most abundant species and is plotted on an $x$ axis of 0 %–100 %. **(b)** *N. incompta* and the following species are plotted on an $x$ axis of 0 %–30 %, while **(c)** *G. bulloides* and *G. falconensis* are combined; both are temperate to subpolar species. **(d)** *T. quinqueloba* is a subpolar taxon. **(e)** Total planktics picked from all 131 samples, including those samples with 10 or fewer specimens. **(f)** Benthic $\delta^{18}$O stack of globally distributed benthic records (Lisiecki and Raymo, 2005) plotted against age with key interglacials listed on the right. Orange bars represent intervals with abundant foraminifera, corresponding closely with interglacials. Yellow bars represent weak layers 1 and 1b in diatom ooze (Gales et al., 2023). The graphic lithology is from Gales et al., 2023. The two + symbols in the age column mark the position of the two magnetic reversals that help define the age model used for Site U1523.

wood, 1998; Whitehead and Bohaty, 2003; Taylor-Silva and Riesselman, 2018), which is also recorded by high abundances of both planktic and benthic foraminifera (this study) with U1523 sample ages of ∼ 3.72–3.65 Ma at Site U1523 compared with ages of ∼ 3.74–3.64 Ma in the LR04 stack. Warm-water planktic foraminifera are recorded in 5 of 8 samples through this interval, all interglacials (Gi7, Gi5, Gi3), while the two glacial samples (Gi6, Gi4) do not contain warm-water taxa. This strong correlation between Site U1523 foraminiferal sample ages and correlative levels in the LR04 stack provide an anchor point for the uppermost lower Pliocene portion of Site U1523 age model, while the two paleomagnetic datums anchor the lower Pleistocene. Above 21.7 m b.s.f. (1.78 Ma), the sedimentation rate decreases from 3.352 to 1.219 cm kyr$^{-1}$, perhaps indicating a change to colder, drier, and less biologically productive conditions in the Ross Sea during the mid to Late Pleistocene (Naish et al., 2009; McKay et al., 2012a). There is also an increase in grain size suggestive of periods of enhanced winnowing (Fig. 4). However, a linear age model from the C1r.3r/C2n tie point to the top of the core implies that peak foraminiferal abundance at 1.63–1.54 m is ∼ 133–126 ka, which aligns well with the age of MIS 5e at 130–123 ka in the LR04 stack. We conclude that the assumption of the linear age–depth model for Site U1523 with a single change in slope at the upper paleomagnetic reversal dated at 1.78 Ma provides a robust first-order control, although we acknowledge the limitations of four control points, two paleomagnetic reversals, and two paleoclimatic events, means it is not a unique solution and our correlations with specific Marine Isotope Stage (MIS) glacial or interglacial intervals from the LR04 stack are best estimates.

### 3.3 Benthic biofacies

A combined Q-mode and R-mode cluster analysis reveals eight benthic foraminiferal biofacies dominated or co-dominated by *Globocassidulina* spp. (especially *G. subglo-*

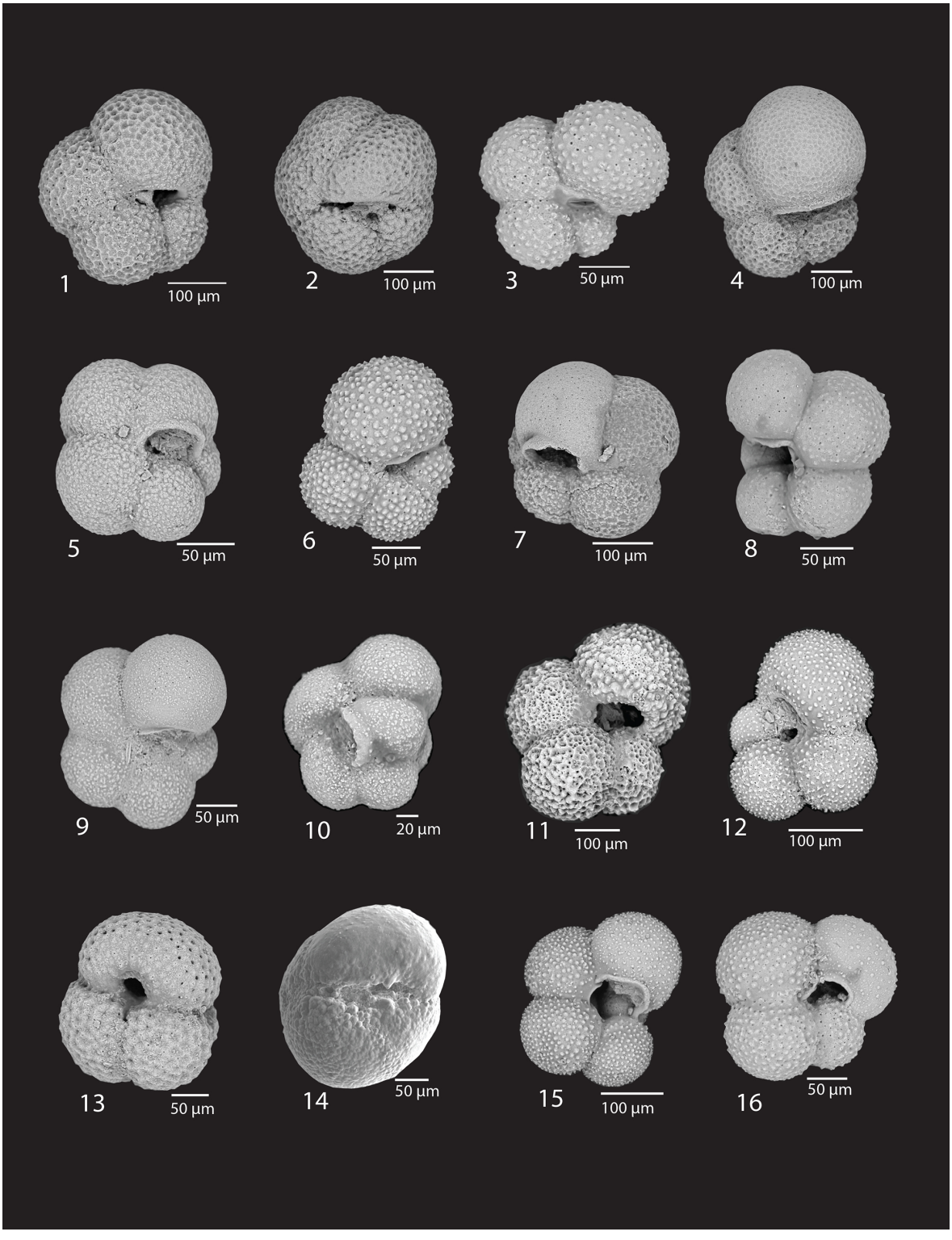


**Plate 1.** (1–6) *Neogloboquadrina pachyderma* (Ehrenberg), U1523A-1H-2, 3–4 cm, U1523A-1H-2, 13–15 cm, U1523A-3H-7, 15–17 cm, U1523A-2H-6, 5–7 cm, U1523B-11F-2, 35–37 cm, U1523A-4F-1, 35–37 cm; (7–8) *Neogloboquadrina incompta* (Cifelli), U1523A-1H-2, 13–15 cm, U1523A-3H-7, 15–17 cm; (9–10) *Turborotalita quinqueloba* (Natland), U1523B-11F-2, 9–10 cm; U1523B-11F-1, 35–37 cm; (11–12) *Globigerina bulloides* d'Orbigny, U1523A-6F-3, 15–17 cm; 35–37; (13) *Globigerinoides ruber* (d'Orbigny), U1523B-5F-3, 35–37 cm; (14) *Globoconella inflata* d'Orbigny, Type II subpolar genotype (Morard et al.), U1523B-5F-3, 35–37 cm, oblique umbilical view; 15–16. *Globigerina falconensis* Blow, U1523A-4F-1, 35–37 cm, U1523A-3H-7, 15–17 cm.

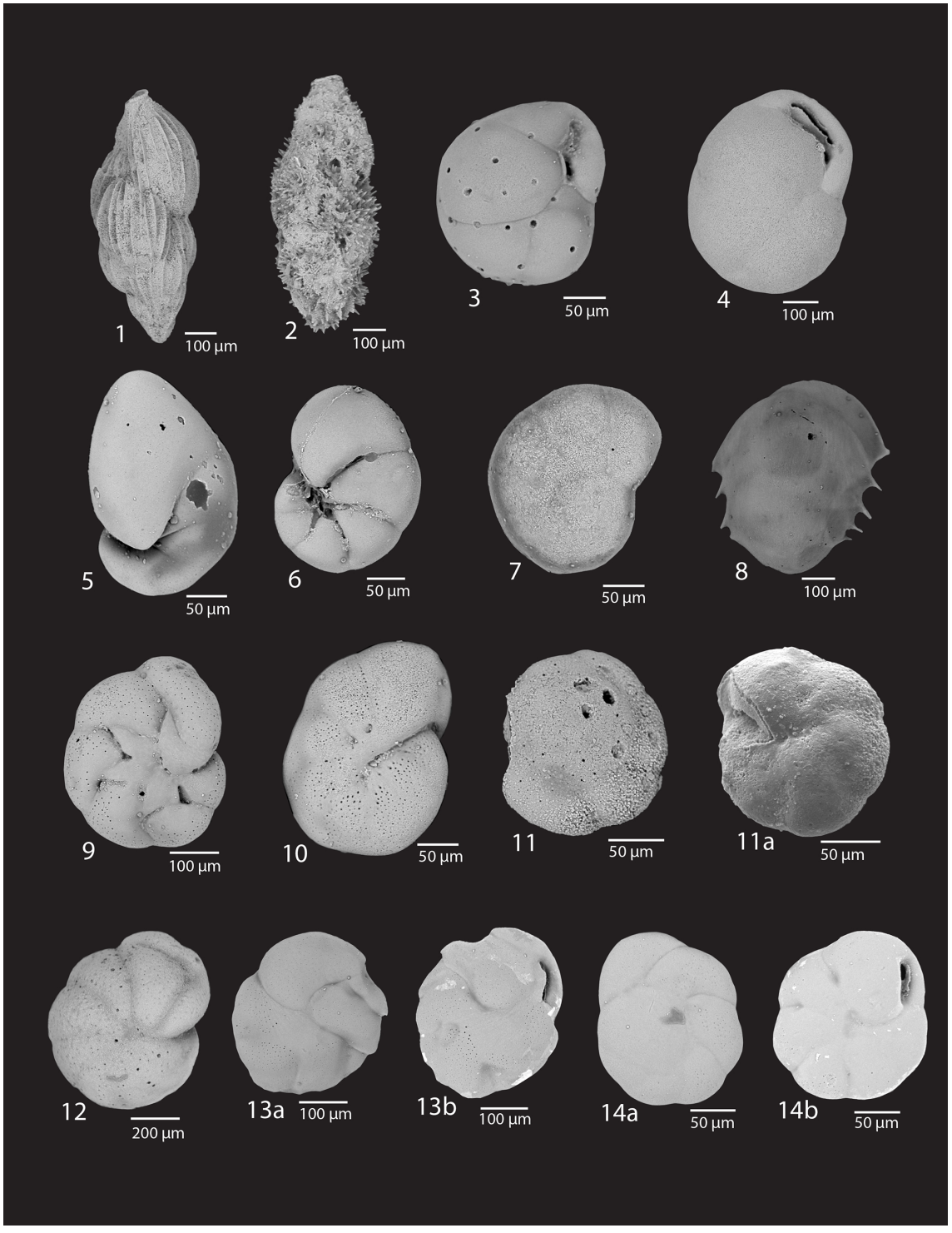


**Plate 2.** (1) *Trifarina earlandi* (Parr), U1523A-1H-1, 17-19 cm; (2) *Trifarina earlandi* (Parr), spinose morphotype, U1523A-1H-1, 17–19 cm; (3) *Globocassidulina subglobosa* (Brady), U1523A-1H-1, 17–19 cm; (4) *Globocassidulina biora* (Crespin), U1523B-5F-1, 110–112 cm; (5) *Nonionella bradii* (Chapman), U1523A-2H-7, 17–19 cm; (6) *Nonionella iridea* Herron–Allen and Earland, U1523A-2H-7, 17–19 cm; (7) *Rosalina globularis* d'Orbigny, U1523A-2H-7, 17–19 cm; (8) *Ehrenbergina glabra* Cushman, U1523A-1H-2, 3–4 cm; (9) *Astrononion antarcticus* Parr, U1523A-1H-2, 13–15 cm; (10) *Astrononion echolsi* Kennett, U1523A-1H-2, 13–15 cm; (11a, b) *Alabaminella weddellensis* Earland, U1523A-1H-1, 17–19 cm; (12) *Cibicides lobatulus* (Walker and Jacob), U1523A-2H-4, 42–44 cm; (13a, b) *Cassidulina teretis* Tappan, U1523A-1H-2, 3–4 cm; (14a, b) *Epistominella vitrea* Parker, U1523A-1H-2, 3–4 cm.

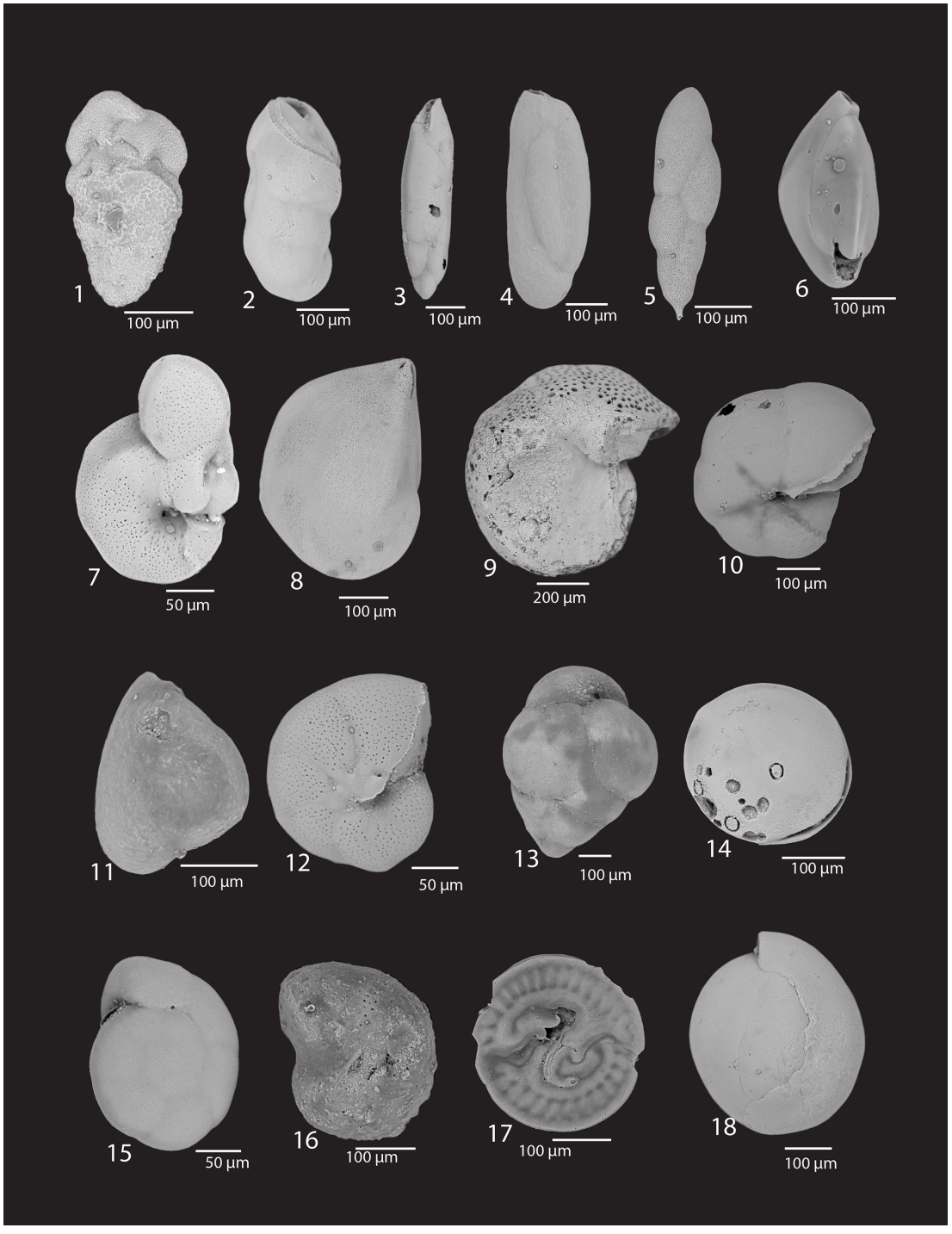


**Plate 3.** (1) *Bolivina* sp., U1523A-6F-2, 15–17 cm; (2) *Cassidulinoides porrectus* (Heron-Allen and Earland), U1523A-3H-7, 90–92 cm; (3) *Fursenkoina fusiformis* (Cushman), U1523B-5F-2, 110–112 cm; (4) *Miliammina arenacea* (Chapman), U1523B-10F-4, 30–32 cm; (5) *Stainforthia concave* (Höglund), U1523A-1H-2, 13–15 cm; (6) *Triloculina* sp., U1523A-2H-7, 23–25 cm; (7) *Melonis barleeanus* Williamson, aberrant specimen, U1523A-5F-1, 15–17 cm; (8) *Lenticulina* sp., Lamarck, 1804, U1523A-3H-7, 90–92 cm; (9) *Cibicides* sp., U1523E-15F-2, 35–37 cm; (10) *Pullenia subcarinata* (d'Orbigny), U1523A-6F-3, 23–27 cm; (11) *Miliammina* sp., Heron-Allen and Earland, U1523B-5F-1, 110–112 cm; (12) *Astrononion echolsi* Kennett,1523A-1H-1, 17–19 cm; (13) *Eggerella bradyi nitens* (Wiesner), U1523A-1H-2, 3–4 cm; (14) Unidentified Nodosariidae, Ehrenberg, U1523A-1H-2, 3–4 cm; (15) *Gyroidina* sp., U1523A-1H-2, 13–15 cm; (16) *Melonis cf. barleeanus* Williamson, U1523A-1H-2, 23–25 cm; (17) *Patellina corrugata* Williamson, U1523A-1H-2, 3–4 cm; (18) *Triloculina* sp., U1523B-11F-1, 35–37 cm.

**Table 1.** Subset of foraminiferal data from U1523 showing samples with 10 or more specimens of planktic and benthic foraminifera (raw data from the 131 samples investigated can be found on https://sciencebase.gov, last access: 28 June 2024). Cluster analysis is based on the 42 samples (32 % of total) with 40 or more specimens of benthic foraminifera (samples in bold). Data counts are provided for the two most common genera of benthic foraminifera, *Globocassidulina* and *Trifarina*, and the two most common species, *G. subglobosa* and *T. earlandi*, as well as all the species of planktic foraminifera identified in this study. Pink-colored boxes correspond with occurrences of warmer-water species: *Globigerina bulloides* + *G. falconensis*, *Globigerinita glutinata, Turborotalita quinqueloba, Globoconella inflata*, and *Globigerinoides ruber*. Dark blue boxes record samples with greater than or equal to 45 % *G. subglobosa* and light blue > 30 % *G. subglobosa*, while dark green boxes record samples with greater than or equal to 45 % *T. earlandi* and light green > 30 % *T. earlandi*. Marine Isotope Stage (MIS) ages are from Lisiecki and Raymo (2005), where red indicates interglacial (I) intervals and blue glacial (G) intervals. The four horizontal black lines show the two paleomagnetic tie points and two paleoclimate (MIS) events used in the age model. **(a)** Uppermost anchor point in age model: U1523 age = 0.126 Ma at 1.54 m CSF-B; MIS 5e age of LR04 stack = 0.123 Ma. **(b)** Big change in benthic foraminifera biofacies. **(c)** Last of the warmer-water planktic species (~ 1.82 Ma), also showing decrease in sedimentation rates from 3.35 to 1.22 cm kyr$^{-1}$ and increased flow of ASC and winnowing. **(d)** Base of Unit I. **(e)** Top of Unit II. **(f)** *G. ruber* + *G. inflata* (and *G. biora*); we suspect that this sample correlates with MIS G17 (see discussion in the main text). **(g)** MIS Gi3 + Gi5 + Gi7 indicates a well-known warm interval in the Southern Ocean that anchors the lower portion of the age model. **(h)** Basal anchor point in age model: U1523 age = 3.721 Ma at 86.75 m CSF-B; MIS Gi7 age of LR04 stack = 3.72 Ma.

| Cruise | Hole | Core | Section | cm top | cm bottom | Top depth CSF-B (m) | Revised Age Model 6/22 | *Globocassidulina biora* | *Globocassidulina subglobosa* | % *Globocassidulina subglobosa* | *Trifarina earlandi* | % *Trifarina earlandi* | *Trifarina earlandi spinose* | Total Benthics | *Turborotalita quinqueloba* | *Globigerina bulloides* + *G. falconensis* | *Globigerinita glutinata* | *Globoratalia inflata* | *Globigerinoides ruber* | *Neogloboquadrina incompta* | % *N. incompta* | *Neogloboquadrina pachyderma* | % *N. pachyderma* | Total Planktics | Glacial (G) or Interglacial (I) | Marine Isotope Stage | Notes |
|---|---|---|---|---|---|---|---|---|---|---|---|---|---|---|---|---|---|---|---|---|---|---|---|---|---|---|---|
| 374 | U1523A | 1H | 1 | 17 | 19 | 0.17 | 0.014 | | 3 | 3.8 | 52 | 65.8 | ∞ | 79 | | | | | | | 0.0 | 49 | 100.0 | 49 | I | 1 | |
| 374 | U1523A | 1H | 1 | 88 | 90 | 0.88 | 0.072 | 1 | 11 | 17.2 | 34 | 53.1 | | 64 | | | | | | 6 | 4.7 | 123 | 95.3 | 129 | I | 5.1 | |
| 374 | U1523A | 1H | 2 | 3 | 4 | 1.54 | 0.126 | | 13 | 8.3 | 84 | 53.8 | | 156 | | | | | | 3 | 2.2 | 133 | 97.8 | 136 | I | 5.5 | A |
| 374 | U1523A | 1H | 2 | 13 | 15 | 1.63 | 0.133 | 5 | 15 | 8.1 | 94 | 50.8 | 1 | 185 | | | | | | 7 | 4.8 | 138 | 95.2 | 145 | G | 6 | |
| 374 | U1523A | 1H | 2 | 23 | 25 | 1.73 | 0.142 | | 9 | 4.2 | 103 | 48.6 | | 212 | | | | | | 6 | 6.4 | 88 | 93.6 | 94 | G | 6 | |
| 374 | U1523A | 1H | 2 | 88 | 90 | 2.38 | 0.195 | 2 | 8 | 7.6 | 50 | 47.6 | | 105 | | | | | | 1 | 0.8 | 121 | 99.2 | 122 | I | 7 | |
| 374 | U1523A | 1H | 3 | 17 | 19 | 3.17 | 0.260 | 2 | | 0.0 | 9 | 36.0 | | 25 | | | | | | | 0.0 | 15 | 100.0 | 15 | G | 8 | |
| 374 | U1523A | 1H | 3 | 88 | 90 | 3.88 | 0.318 | | 1 | 5.6 | 15 | 83.3 | | 18 | | | | | | | 0.0 | 22 | 100.0 | 22 | I | 9 | |
| 374 | U1523A | 1H | 4 | 13 | 15 | 4.64 | 0.380 | | 2 | 4.7 | 26 | 60.5 | | 43 | | | | | | 1 | 3.7 | 26 | 96.3 | 27 | I | 11 | |
| 374 | U1523A | 1H | 5 | 47 | 49 | 6.43 | 0.527 | | 1 | 3.0 | 28 | 84.8 | | 33 | | | | | | | 0.0 | 21 | 100.0 | 21 | I | 13 | |
| 374 | U1523A | 1H | 5 | 73 | 75 | 6.73 | 0.552 | | 6 | 9.7 | 46 | 74.2 | | 62 | | | | | | 5 | 2.4 | 202 | 97.6 | 207 | G | 14 | |
| 374 | U1523A | 1H | 5 | 103 | 105 | 7.03 | 0.577 | | | 0.0 | 6 | 75.0 | | 8 | | | | | | | 0.0 | 11 | 100.0 | 11 | I | 15 | |
| 374 | U1523A | 1H | 5 | 137 | 139 | 7.33 | 0.601 | | 4 | 25.0 | 10 | 62.5 | | 16 | | | | | | 4 | 9.8 | 37 | 90.2 | 41 | I | 15 | |
| 374 | U1523A | 1H | CC | 23 | 28 | 8.47 | 0.695 | | 3 | 15.8 | 6 | 31.6 | | 19 | | | | | | 1 | 10.0 | 9 | 90.0 | 10 | I | 17 | |
| 374 | U1523A | 2H | 3 | 17 | 19 | 11.68 | 0.958 | | | 0.0 | 4 | 25.0 | | 16 | | | | | | 2 | 1.3 | 157 | 98.7 | 159 | I | 25 | |
| 374 | U1523A | 2H | 3 | 88 | 90 | 12.39 | 1.016 | | 4 | 28.6 | 3 | 21.4 | | 14 | | | | | | | 0.0 | | 0.0 | 0 | I | 29 | |
| 374 | U1523A | 2H | 3 | 125 | 127 | 12.76 | 1.047 | | 3 | 7.5 | 7 | 17.5 | | 40 | | | | | | 9 | 3.4 | 252 | 96.6 | 261 | G | 30 | |
| 374 | U1523A | 2H | 4 | 17 | 19 | 13.18 | 1.081 | | 7 | 14.0 | 5 | 10.0 | | 50 | | | | | | 4 | 1.5 | 268 | 98.5 | 272 | I | 31-32 | |
| 374 | U1523A | 2H | 4 | 42 | 44 | 13.46 | 1.104 | | | 0.0 | 19 | 45.2 | | 42 | | | | | | 7 | 2.7 | 249 | 97.3 | 256 | I | 32-33 | |
| 374 | U1523A | 2H | 4 | 92 | 94 | 13.93 | 1.143 | | 6 | 9.0 | 14 | 20.9 | | 67 | | | | | | 4 | 1.6 | 242 | 98.4 | 246 | I | 35 | |
| 374 | U1523A | 2H | 4 | 111 | 113 | 14.16 | 1.161 | 1 | 5 | 9.1 | 28 | 50.9 | | 55 | | | | | | 9 | 3.5 | 246 | 96.5 | 255 | I | 35 | |
| 374 | U1523A | 2H | 4 | 126 | 128 | 14.26 | 1.170 | | 6 | 14.0 | 7 | 16.3 | | 43 | | | | | | 8 | 2.9 | 269 | 97.1 | 277 | I | 35 | |
| 374 | U1523A | 2H | 4 | 133 | 134 | 14.36 | 1.178 | | 4 | 7.5 | 25 | 47.2 | | 53 | | | | | | 12 | 5.0 | 229 | 95.0 | 241 | I | 35 | |
| 374 | U1523A | 2H | 4 | 143 | 145 | 14.46 | 1.186 | | 3 | 5.6 | 17 | 31.5 | | 54 | | | | | | 8 | 3.1 | 250 | 96.9 | 258 | I | 35 | |
| 374 | U1523A | 2H | 5 | 9 | 11 | 14.57 | 1.195 | 1 | 6 | 17.1 | 9 | 25.7 | | 35 | | | | | | 14 | 5.3 | 251 | 94.7 | 265 | G | 36 | |
| 374 | U1523A | 2H | 5 | 17 | 19 | 14.69 | 1.205 | | 6 | 10.7 | 11 | 19.6 | | 56 | | | | | | 8 | 2.9 | 270 | 97.1 | 278 | G | 36 | |
| 374 | U1523A | 2H | 6 | 5 | 7 | 14.79 | 1.213 | 2 | | 0.0 | 14 | 23.3 | | 60 | | | | | | 8 | 3.3 | 235 | 96.7 | 243 | G | 36 | |
| 374 | U1523A | 2H | 6 | 17 | 19 | 14.91 | 1.223 | | 8 | 13.3 | 22 | 36.7 | | 60 | | | | | | 9 | 3.3 | 261 | 96.7 | 270 | I | 37 | |
| 374 | U1523A | 2H | 6 | 26 | 28 | 14.99 | 1.230 | 1 | 1 | 3.7 | 8 | 29.6 | | 27 | | | | | | 5 | 1.8 | 276 | 98.2 | 281 | I | 37 | |
| 374 | U1523A | 2H | 7 | 5 | 7 | 15.13 | 1.241 | 1 | 2 | 28.6 | | 0.0 | | 7 | | | | | | 1 | 4.5 | 21 | 95.5 | 22 | I | 37 | |
| 374 | U1523A | 2H | 7 | 17 | 19 | 15.25 | 1.251 | | 5 | 10.0 | 9 | 18.0 | | 50 | | | | | | 7 | 2.7 | 248 | 97.3 | 255 | G | 38 | |
| 374 | U1523A | 2H | 7 | 23 | 25 | 15.33 | 1.257 | | 8 | 12.3 | 21 | 32.3 | | 65 | | | | | | 7 | 2.7 | 250 | 97.3 | 257 | G | 38 | |
| 374 | U1523A | 2H | 7 | 71 | 73 | 15.79 | 1.295 | | 5 | 11.4 | 19 | 43.2 | | 44 | | | | | | 7 | 2.4 | 279 | 97.6 | 286 | G | 40 | |
| 374 | U1523A | 2H | CC | 12 | 17 | 15.98 | 1.311 | 1 | 2 | 8.7 | 10 | 43.5 | | 23 | | | | | | 3 | 2.6 | 111 | 97.4 | 114 | I | 41 | |
| 374 | U1523A | 3H | 1 | 15 | 17 | 18.15 | 1.489 | 6 | 53 | 37.6 | 60 | 42.6 | | 141 | | | | | | 1 | 0.6 | 174 | 99.4 | 175 | I | 49 | B |
| 374 | U1523A | 3H | 1 | 90 | 92 | 18.90 | 1.550 | | 31 | 49.2 | 25 | 39.7 | | 63 | | | | | | 1 | 1.1 | 92 | 98.9 | 93 | I | 53 | |
| 374 | U1523A | 3H | 2 | 90 | 92 | 20.24 | 1.660 | | 63 | 44.7 | 47 | 33.3 | | 141 | | | | | | 4 | 2.2 | 177 | 97.8 | 181 | G | 58 | |
| 374 | U1523A | 3H | 3 | 15 | 17 | 20.50 | 1.682 | | 30 | 47.6 | 15 | 23.8 | | 63 | | | | | | 4 | 3.8 | 100 | 96.2 | 104 | I | 59 | |
| 374 | U1523A | 3H | 6 | 15 | 17 | 22.93 | 1.817 | 1 | 36 | 39.6 | 41 | 45.1 | | 91 | | 6 | | | | 1 | 0.5 | 207 | 96.7 | 214 | G | 66 | C |
| 374 | U1523A | 3H | 7 | 15 | 17 | 23.53 | 1.834 | | 24 | 32.0 | 29 | 38.7 | | 75 | | 5 | | | | 5 | 2.0 | 245 | 96.1 | 255 | G | 68 | |
| 374 | U1523A | 3H | 7 | 90 | 92 | 24.28 | 1.857 | 1 | 32 | 36.4 | 39 | 44.3 | | 88 | 1 | 1 | | | | 4 | 1.7 | 235 | 97.5 | 241 | I | 69 | |
| 374 | U1523A | 3H | 8 | 15 | 17 | 24.58 | 1.866 | 2 | 31 | 30.4 | 42 | 41.2 | | 102 | | 17 | | | | 4 | 1.6 | 227 | 91.5 | 248 | G | 70 | |
| 374 | U1523A | 3H | CC | 15 | 20 | 25.17 | 1.883 | 19 | 27 | 20.8 | 42 | 32.3 | | 130 | | 6 | | | | 3 | 2.6 | 111 | 97.4 | 114 | I | 71 | |
| 374 | U1523A | 4F | 1 | 35 | 37 | 27.85 | 1.963 | 10 | 26 | 20.0 | 56 | 43.1 | | 130 | | 23 | | | | 4 | 2.1 | 167 | 86.1 | 194 | G | 74 | |
| 374 | U1523A | 4F | 2 | 15 | 17 | 28.16 | 1.973 | 9 | 32 | 22.7 | 56 | 39.7 | | 141 | | 9 | | | | 4 | 2.2 | 165 | 92.7 | 178 | I | 75 | |
| 374 | U1523A | 4F | 2 | 90 | 92 | 28.91 | 1.995 | | 8 | 22.2 | 19 | 52.8 | | 36 | | | | | | 2 | 2.4 | 81 | 97.6 | 83 | G | 76 | |
| 374 | U1523A | 4F | 3 | 15 | 17 | 29.54 | 2.014 | | 2 | 12.5 | 7 | 43.8 | | 16 | | | | | | | 0.0 | 24 | 100.0 | 24 | G | 76 | |
| 374 | U1523A | 4F | CC | 28 | 33 | 30.95 | 2.056 | 4 | 24 | 28.2 | 26 | 30.6 | | 85 | | 2 | | | | 2 | 5.1 | 37 | 94.9 | 39 | G | 78 | |
| 374 | U1523A | 5F | 1 | 15 | 17 | 32.35 | 2.098 | | 30 | 56.6 | 11 | 20.8 | 1 | 53 | | | | | | | 0.0 | 28 | 100.0 | 28 | I | 79 | |
| 374 | U1523A | 5F | 2 | 17 | 19 | 33.15 | 2.121 | 1 | | 0.0 | 2 | 12.5 | | 16 | | | | | | 2 | 20.0 | 8 | 80.0 | 10 | G | 80 | D |
| 374 | U1523A | 6F | 2 | 15 | 17 | 38.54 | 2.282 | | 4 | 28.6 | 2 | 14.3 | | 14 | | | | | | | 0.0 | 34 | 100.0 | 34 | G | 88 | E |
| 374 | U1523A | 6F | 3 | 5 | 7 | 39.93 | 2.324 | | 21 | 30.4 | 32 | 46.4 | | 69 | | 5 | | | | 1 | 0.4 | 228 | 97.4 | 234 | G | 90 | |
| 374 | U1523A | 6F | 3 | 15 | 17 | 40.02 | 2.327 | | 22 | 21.8 | 59 | 58.4 | | 101 | | 13 | 2 | | | 8 | 3.7 | 194 | 89.4 | 217 | G | 90 | |
| 374 | U1523A | 6F | 3 | 23 | 27 | 40.12 | 2.329 | | 10 | 11.1 | 64 | 71.1 | | 90 | | 1 | | | | 1 | 2.6 | 37 | 94.9 | 39 | G | 90 | |
| 374 | U1523A | 6F | CC | 12 | 17 | 41.57 | 2.373 | 2 | 23 | 53.5 | 11 | 25.6 | | 43 | | 4 | | | | 1 | 2.0 | 48 | 98.0 | 49 | I | 92-93 | |
| 374 | U1523B | 3F | 1 | 43 | 45 | 47.05 | 2.536 | | 4 | 21.1 | 9 | 47.4 | | 19 | | | | | | | 0.0 | 23 | 100.0 | 23 | G | 100 | |
| 374 | U1523B | 5F | 1 | 110 | 112 | 57.20 | 2.839 | 11 | 2 | 11.8 | 1 | 5.9 | | 17 | | | | | | | 0.0 | 3 | 100.0 | 3 | G | G12 | |
| 374 | U1523B | 5F | 2 | 110 | 112 | 58.71 | 2.884 | 11 | | 0.0 | | 0.0 | | 23 | | | | | | | 0.0 | 2 | 100.0 | 2 | G | G14 | |
| 374 | U1523B | 5F | 3 | 35 | 37 | 59.48 | 2.907 | 4 | | 0.0 | | 0.0 | | 7 | | | | 6 | 4 | | 0.0 | 9 | 47.4 | 19 | I | G15 | F |
| 374 | U1523B | 7F | 2 | 35 | 37 | 67.31 | 3.141 | | 2 | 66.7 | | 0.0 | | 3 | | | | | | | 0.0 | 14 | 100.0 | 14 | G | KM2 | |
| 374 | U1523B | 9F | 1 | 28 | 30 | 75.18 | 3.375 | | 1 | 4.8 | 7 | 33.3 | | 21 | | | | | | | 0.0 | 7 | 100.0 | 7 | G | MG4 | |
| 374 | U1523E | 15F | 2 | 35 | 37 | 83.55 | 3.625 | | 7 | 24.1 | 12 | 41.4 | | 29 | | | | | | | 0.0 | 31 | 100.0 | 31 | G | GI2 | |
| 374 | U1523B | 10F | 4 | 30 | 32 | 83.65 | 3.628 | | | 0.0 | 1 | 8.3 | | 12 | | | | | | | 0.0 | | 0.0 | 0 | G | GI2 | |
| 374 | U1523B | 10F | CC | 15 | 20 | 84.12 | 3.642 | | 5 | 33.3 | | 0.0 | | 15 | | | | | | | 0.0 | 3 | 100.0 | 3 | I | GI3 | |
| 374 | U1523E | 15F | 2 | 110 | 112 | 84.30 | 3.647 | | 3 | 23.1 | 6 | 46.2 | | 13 | 1 | | | | | | 0.0 | 12 | 92.3 | 13 | I | GI3 | G |
| 374 | U1523B | 11F | 1 | 35 | 37 | 84.65 | 3.658 | 1 | 51 | 56.7 | 8 | 8.9 | | 90 | 19 | | | | | 2 | 0.9 | 202 | 90.6 | 223 | I | GI3 | |
| 374 | U1523B | 11F | 2 | 35 | 37 | 85.24 | 3.675 | | 16 | 53.3 | 4 | 13.3 | | 30 | 18 | 1 | | | | | 0.0 | 52 | 73.2 | 71 | I | GI5 | |
| 374 | U1523B | 11F | 3 | 35 | 37 | 85.94 | 3.696 | | 10 | 52.6 | 4 | 21.1 | | 19 | 6 | | | | | | 0.0 | 19 | 76.0 | 25 | I | GI5 | |
| 374 | U1523B | 11F | CC | 0 | 8 | 86.34 | 3.708 | | 36 | 30.0 | 36 | 30.0 | | 120 | | | | | | | 0.0 | 28 | 100.0 | 28 | G | GI6 | |
| 374 | U1523E | 16F | 1 | 35 | 37 | 86.75 | 3.721 | | 32 | 50.8 | 7 | 11.1 | | 63 | 4 | 2 | | | | 3 | 1.1 | 258 | 96.6 | 267 | I | GI7 | H |
| | | | | | | | | | | 45% | | 45% | | | | | | | | | | | | | | | |
| | | | | | | | | | | 30% | | 30% | | | | | | | | | | | | | | | |

*bosa*) or *Trifarina earlandi* with accessory taxa characteristic of particular biofacies. In general, *G. subglobosa* biofacies clusters dominate before ∼ 1.5 Ma (red, orange, and yellow; Figs. 6 and 7), while *T. earlandi* biofacies become dominant after ∼ 1.5 Ma (blue, brown, purple, and green). *Trifarina earlandi* co-dominates with *Globocassidulina subglobosa* in the orange and yellow biofacies, while *Gavelinopsis* is an accessory taxon in the lime green biofacies. *Globocassidulina biora – Epistominella – Nonionella* defines a unique gold biofacies at ∼ 2.88 Ma. Accessory taxa with *T. earlandi* include *Rosalina* and *Nonionella* in the green biofacies. The latter biofacies (green) characterizes a narrow interval of the Mid-Pleistocene correlative with MIS 37 to MIS 31 (∼ 1.23–1.07 Ma).

## 4 Discussion

### 4.1 Preservation of calcareous foraminifera

Foraminiferal assemblages are generally dominated by planktic species (Fig. 4e) through much of the Pleistocene at Site U1523, although there is a stepped increase in the percent benthics during the late Early Pleistocene through the Mid-Pleistocene Transition (Fig. 4; MIS 77 to MIS 31; ∼ 2.0 to 1.0 Ma) and then again at the MIS 6–5e transition in the Late Pleistocene. Foraminiferal abundances vary greatly through the Pliocene–Pleistocene section. Polar oceans have lower calcium carbonate saturation states ($\Omega = [CO_3^{2-}] \times [Ca^{2+}] / K^*_{sp}$) due in part to the higher stoichiometric solubility product ($K^*_{sp}$) as a function of lower temperature (e.g., Azetsu-Scott et al., 2010). Low foraminiferal abundances and frequent barren samples in the diatom-rich upper Pliocene–lower Pleistocene interval (Fig. 9; MIS Gi3 to MIS 91; ∼ 3.65 to 2.4 Ma) may be a consequence of carbonate dissolution due to a high flux of organic matter associated with generally open marine conditions during deposition of diatom-bearing or diatom-rich Unit II sediments. Hauck et al. (2012) compiled carbonate saturation values ($\Omega_{calcite}$) from GLODAP and CARINA data on the continental shelf and slope of Antarctica, revealing that all Antarctic shelf waters today are saturated with respect to calcite ($\Omega_{calcite} => 1.3$; undersaturated $< 1$; saturated $> 1$). However, the calcite saturation state can decrease significantly under areas of high productivity (Emerson and Bender, 1981) where dissolved inorganic carbon (DIC) values in the upper 1 cm of the sediments can increase 100 to 200 µmol $kg^{-1}$ due to the remineralization of organic matter (Sachs et al., 2009; Hauck et al., 2013). Hauck et al. (2013) demonstrated how increased flux of organic matter and oxidative remineralization of the organic matter (OM) on the Antarctic shelf causes calcite undersaturation and metabolic-$CO_2$-driven dissolution of calcite in the upper layers of the sediments. This is a serious syn- to post-depositional problem for carbonate preservation in diatom-rich sediments of the Ross Sea.

Alternatively, dissolution of calcareous foraminifera may be due to the production of corrosive High Saline Shelf Water (HSSW) associated with sea ice formation and brine rejection in the Ross Sea polynya (e.g., Osterman and Kellogg, 1979; Melis and Salvi, 2009; Majewski et al., 2016, 2018, 2020; Capotondi et al., 2018; Prothro et al., 2018; Kim et al., 2020). Another hypothesis is dilution by high sedimentation rates, although there does not appear to be a pattern of changing sedimentation rates in the U1523 study interval. Conte et al. (2021) observed a decrease in the sedimentation rate and bottom current strength during the deposition of the seismic unit RSS-6 correlated with sediments at depths of ∼ 60–100 m b.s.f. in Site U1523. They infer that the production of dense waters on the continental shelf was generally reduced and the Antarctic Slope Front was very weak during the warm climate phase of the mid-Pliocene Warm Period (3.3–3 Ma).1

What is dissatisfying about the dissolution hypotheses (dissolution due to biosiliceous productivity and flux of organic matter to the seafloor versus corrosive HSSW) is the absence of agglutinated foraminifera in Unit II sediments. A further possibility for the paucity of foraminifera in many Unit II samples, including agglutinated taxa, is perennial sea ice cover that would have limited productivity and the organic flux required for benthic foraminifera. Such conditions may have been associated with Southern Ocean cooling during the Late Pliocene to Early Pleistocene, ∼ 3.59 or 3.5 to ∼ 2.5 Ma, including the M2 glaciation (Patterson et al., 2014; Tagliaro et al., 2022) and roughly corresponding with a 44 m thick interval at Site U1523 (∼ 84 to 40 m b.s.f.; ∼ 3.6 to 2.4 Ma) with very low abundances of foraminifera (Fig. 4); maybe this is more than coincidental. However, the ∼ 1.2 Myr interval at Site U1523 is interrupted by open marine, diatomaceous, super-interglacials, including MIS G17 (∼ 2.95 Ma), and a second interval that likely correlates with MIS KM3 (∼ 3.16 Ma) of the mid-Piacenzian Warm Period (Dowsett et al., 2011; Raymo et al., 2011). These two diatom-rich intervals at Site U1523 correspond with weak layers WL-1b and WL-1, respectively (Gales et al., 2023). The incursion of CDW and mCDW into the Ross Sea during the Pliocene may have supplied nutrients, including dissolved iron, to support biosiliceous productivity (e.g., Castagno et al., 2017; Capotondi et al., 2018). Carbonate dissolution in the biosiliceous sediments may have further exacerbated the long Late Pliocene–Early Pleistocene interval with so few foraminifera.

### 4.2 Benthic foraminiferal biofacies and Ross Sea water masses

The most common benthic species at Site U1523 are plotted in Fig. 6. These species include *Trifarina earlandi* (= *T. angulosa* of other authors) and *Globocassidulina subglobosa*, followed by *Nonionella iridea, Rosalina globularis, Ehrenbergina glabra, Astrononion* spp., *Alabaminella*

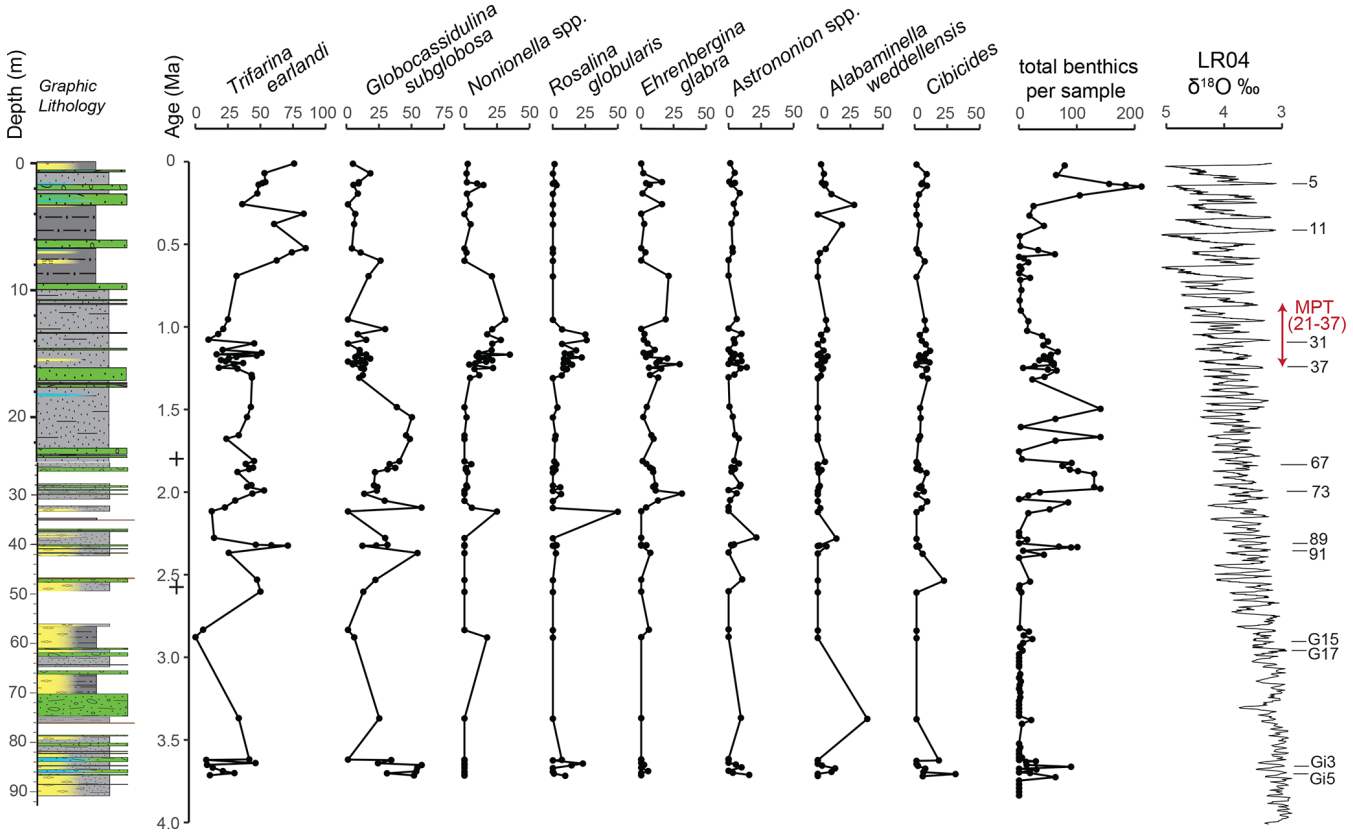


**Figure 6.** Relative abundance of the major benthic foraminiferal species in U1523 plotted against age (Ma). Relative abundances for **(a)**–**(h)** were only plotted if there were more than 10 specimens in the sample ($n = 66$); all other samples were excluded. **(a)** *Trifarina earlandi* is the most common species and is plotted on an $x$ axis of 0 %–100 %. **(b)** *Globocassidulina subglobosa* is plotted on an $x$ axis of 0 %–75 %. **(c)** *Nonionella* includes *N. iridea* and *N. bradii*, and the following species are plotted on an $x$ axis of 0 %–50 %: **(d)** *Rosalina globularis*, **(e)** *Ehrenbergina glabra*, **(f)** *Astrononion* including *A. antarcticum* and *A. echolsi*, **(g)** *Alabaminella weddellensis*, and **(h)** *Cibicides* including *C. lobatulus* and *C. refulgens*. **(i)** Total benthics picked from all 131 samples including those samples with 10 or fewer specimens. **(j)** Benthic $\delta^{18}$O stack of globally distributed benthic records (Lisiecki and Raymo, 2005) plotted against age, with key interglacials listed on the right. The graphic lithology is from Gales et al. (2023).

*weddellensis*, and *Cibicides lobatulus*. Very rare specimens of *Eggerella* sp., *Miliammina arenacea*, and *Haplophragmoides* sp. are the only agglutinated species found at Site U1523. A combined Q-mode and R-mode cluster analysis reveals eight biofacies dominated or co-dominated by *T. earlandi* and/or *G. subglobosa*. A significant change in benthic foraminiferal biofacies after ∼ 1.5 Ma (MIS 49), prior to the Mid-Pleistocene Transition.

*Trifarina earlandi* is the most common benthic taxon in this study. The *Trifarina earlandi* biofacies (blue, brown, purple, and green; Figs. 6, 7; Table 1) are indicative of the continental shelf break and upper slope with stronger bottom water currents (Osterman and Kellogg, 1979; Melis and Salvi, 2009; Majewski et al., 2018). Ishman and Szymcek (2003) show that *Trifarina earlandi* (as *Angulogerina earlandi*) is found in winnowing conditions associated with ice edge environments, which are sandier than other facies, and low in total organic carbon (TOC) and diatom abundance. In addition to their association with active bottom water circulation, Uvigerinids, including *Trifarina*, are known to be shallow infaunal taxa that may correlate with high accumulation rates of organic matter and high productivity (e.g., Gooday, 2003; Jorissen et al., 2007; Diester-Haass et al., 2018).

*Trifarina earlandi* is found to be associated with both glacial and interglacial intervals (Table 1). *Trifarina earlandi* has relative abundances of > 45 % in 22 of the 66 samples with at least 10 benthic specimens (33.3 %) and relative abundance of > 30 % in 43 of these samples (65.1 %); 12 of the 22 samples (54.5 %) with the highest relative abundances of *T. earlandi* are associated with interglacial intervals and 10 are associated with glacials (45.5 %) based on our age model. However, we note that samples older than ∼ 1.82 Ma show a strong correlation of high *T. earlandi* abundances with glacials (85.7 %), whereas samples younger than ∼ 1.82 Ma show a stronger correlation with interglacial intervals (80 %).

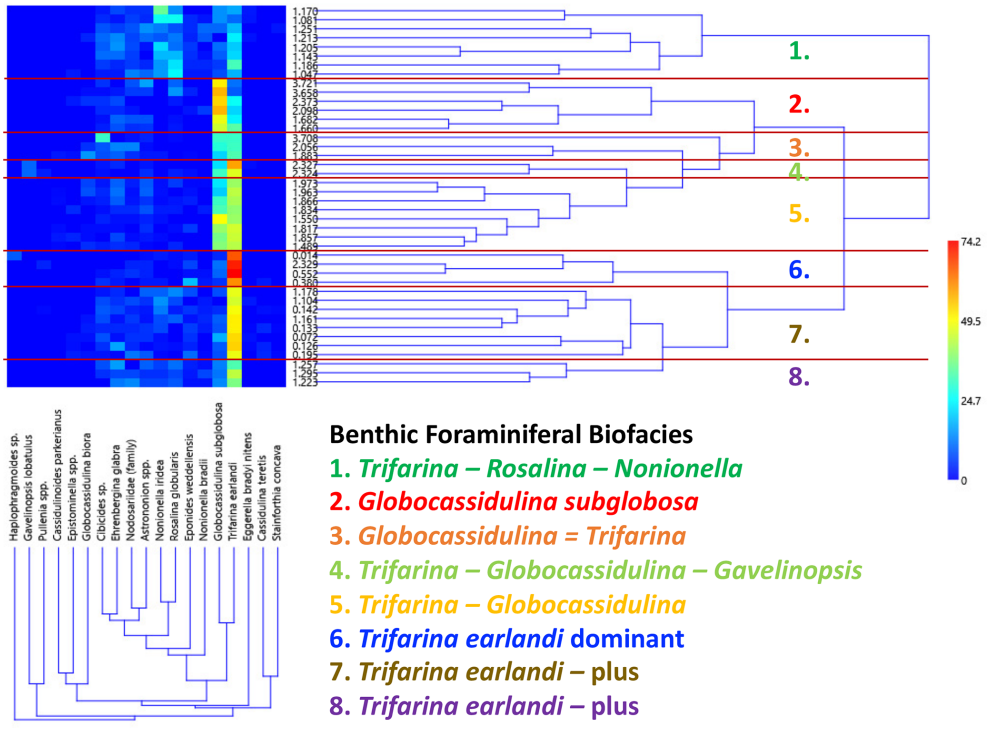


**Figure 7.** Q-mode and R-mode combined cluster analysis using PAST and the Bray–Curtis similarity index. This analysis includes samples with 40 or more specimens (N=42). The two dominant taxa are *Trifarina earlandi* and *Globocassidulina subglobosa*. See the discussion in the text.

This observation suggests that the glacial intervals prior to ∼ 1.82 Ma had strong currents and/or high productivity along the shelf break, but current strength and/or productivity was weaker during interglacials (Fig. 9). After ∼ 1.82 Ma, current velocities increased significantly during interglacials, particularly after the MPT. For example, during the past 600 kyr, *T. earlandi* averages 52.4 % in four glacial samples and 65.1 % in nine interglacial samples. We note that 1.82 Ma also marks the end of warmer-water planktic foraminifera occurrences at Site U1523, likely attributable to strengthening meridional temperature gradients, wind speeds, and ACC velocity, resulting in a stronger ASC during both glacial and interglacial times. The decrease in sedimentation rate after 1.78 Ma (Fig. 2) and decrease in mud (< 63 µm) after ∼ 1.5 Ma (Fig. 4) both support an increase in ASC velocity along the shelf break causing the winnowing of finer-grained sediments. We hypothesize that variable changes in current velocity on the shelf, and particularly along the shelf break, can be tracked by changes in percent abundance of *Trifarina*, and these current changes are likely to regulate shifts in water mass exchange at the continental shelf break. The ACC was stronger during interglacials (Lamy et al., 2024). The big increase in *Trifarina* at MIS 5e and other interglacials supports this. Many of the warm intervals at Site U1523 correspond with peaks in ACC strength. Faster, stronger ACC during warmer intervals may also mean a stronger Ross Gyre and Antarctic Slope Current, which may have transported warmer-water planktic foraminifers into the Ross Sea. Increased abundances of *Trifarina earlandi* at Site U1523 coincide with stronger flow of the ASC along the shelf break (also increased Ross Gyre means increased SW transport of warmer CDW; see Nakayama et al., 2018.)

*Globocassidulina subglobosa* is the second most common benthic species in this study and has been a common, widespread deep-sea taxon (1500–4000 m; Hayward et al., 2007) since the Early Eocene (e.g., Mackensen and Berggren, 1992). It has been linked to Indian Deep Water and upper Antarctic Bottom Water in the Indian Ocean (Corliss, 1979; Peterson, 1984), North Atlantic Deep Water in the southwestern Indian Ocean (Corliss, 1983) and South Atlantic Ocean (Peterson and Lohmann, 1982; Mackensen et al., 1995; Schmiedl and Mackensen, 1997), and Circumpolar Deep Water in the southwestern Atlantic (Hodell et al., 1983) and southwestern Pacific (Hayward et al., 2007). For example, in a study of 43 core tops in the equatorial Indian Ocean, Peterson (1984) showed that *Globocassidulina subglobosa* dominates abyssal benthic foraminifera assemblages shallower than 3800 m where carbonate saturation values are > 1.0 and the calcite dissolution index is low, whereas *Nuttallides umbonifera* dominates assemblages deeper than 3800 m where carbonate saturation values are < 1.0 and calcite dissolution is high.

*Globocassidulina subglobosa* invaded the continental shelf of the Ross Sea as Antarctica became increasingly glaciated during the Oligocene and Early Miocene (Leckie and Webb, 1983, 1986; Webb et al., 1986; Coccioni and Galeotti, 1997; Strong and Webb, 2000, 2001; Webb and Strong, 2006; Patterson and Ishman, 2012; Bombard et al., 2024); it is one of the most common calcareous benthic foraminiferal species in the Ross Sea throughout the Neogene and Quaternary (e.g., Bombard et al., 2024; this study). Milam and Anderson (1981) noted that some modern species are found at shallower depths on the Antarctic continental margin compared with lower-latitude occurrences; this high-latitude shoaling of typically deep-water taxa, including *G. subglobosa*, has probably influenced benthic foraminiferal distributions in the Ross Sea since the Oligocene (Webb, 1989; Coccioni and Galeotti, 1997).

The relative abundances of *Globocassidulina subglobosa* are $> 45\,\%$ in 9 of the 66 samples with at least 10 benthic specimens (13.6 %), and there is a relative abundance of $> 30\,\%$ in 16 of these samples (24.2 %); 8 of the 9 samples (88.9 %) with the highest relative abundances of *G. subglobosa* are associated with interglacial intervals (Table 1). In two upper Pleistocene samples, *G. subglobosa* has relative abundances of 25 % or more, and both are from interglacial intervals (MIS 29, MIS 15) based on our age model. *Globocassidulina subglobosa* is most common in the Pliocene–lower Pleistocene interval $> 1.5$ Ma, when the Ross Sea was warmer and not as isolated by a strong ACC and strong Polar Front, particularly in MIS Gi7 to MIS Gi3 ($\sim 3.72$–$3.65$ Ma), a well-known Southern Ocean super-interglacial (Whitehead and Bohaty, 2003; Taylor-Silva and Riesselman, 2018; Conte et al., 2021). The interval $> 1.82$ Ma also has numerous peaks in temperate water planktic species (*Globigerina bulloides*, *G. falconensis*; Fig. 9).

*Globocassidulina subglobosa* is the dominant benthic foraminiferal species proximal to LGM grounding zone wedges in the western Ross Sea (Bart et al., 2016; Prothero et al., 2018; Majewski et al., 2018, 2020). *Globocassidulina biora* is endemic to the Antarctic continental shelf, and like its ancestor *G. subglobosa* in the western Ross Sea, *G. biora* is characteristic of sub-ice-shelf conditions, proximal to retreating LGM grounding zone wedges in the eastern Ross Sea (Majewski et al., 2016, 2018, 2021). These distinctive landforms record the stepwise retreat of the grounded ice sheet since the LGM. The retreat of the grounded LGM ice sheets in the Ross Sea, and the basal melting and thinning of ice shelves observed today is facilitated by the incursion of CDW and mCDW onto the continental shelf (e.g., Pritchard et al., 2012; Capotondi et al., 2018; Prothero et al., 2018; Smith et al., 2019; Conte et al., 2021). The strong association of *Globocassidulina* spp. with sub-ice-shelf facies proximal and distal to grounding zone wedges is a primary reason why we interpret *G. subglobosa* and *G. biora* as proxies of CDW and mCDW incursion into the Ross Sea. This hypothesis is further supported by Hillenbrand et al. (2017), who show that *Globocassidulina* spp. are the dominant taxa during early Holocene warming and ice shelf retreat ($\sim 10.4$–$7.5$ ka) in the Amundsen Sea embayment, as marked by low $\delta^{13}C_{benthic}$ values (older water mass, higher nutrients) and higher Mg and Ca values (warmer paleotemperatures), which are both indicative of CDW. In the Hillenbrand et al. (2017) study, *Globocassidulina* dominance (CDW proxy) is replaced by *Trifarina earlandi* in a pattern reminiscent of the alternating pattern of *Globocassidulina* and *Trifarina* (or *Uvigerina*) dominance throughout the Neogene and Quaternary of the Ross Sea (Leckie and Webb, 1986; Bombard et al., 2024). We interpret that episodic incursions of CDW and mCDW at Site U1523 were more significant prior to 1.5 Ma based on the dominance of *Globocassidulina subglobosa* (Fig. 6).

*Globocassidulina biora* is a large species that is also associated with strong currents at the seafloor, such as in proximal grounding zone wedges and along the shelf break where the Antarctic Slope Current (ASC) winnows finer biosiliceous sediments to create a coarse, residual glaciomarine facies (Prothro et al., 2018; Majewski et al., 2018, 2020). The much smaller, shallow infaunal *G. subglobosa* has also been associated with elevated bathymetry, strong bottom currents, and sandy sediments (Corliss, 1979; Mackensen et al., 1995; Schmiedl et al., 1997; Gooday, 2003; Hayward et al., 2007; Prothro et al., 2018). A unique *G. biora* assemblage was identified at $\sim 2.88$ Ma (MIS G14), with additional peak occurrences of *G. biora* recorded at $\sim 2.84$ Ma (MIS G12) and 1.97–1.88 Ma (MIS 75–71), corresponding with interglacial and glacial intervals of the latest Pliocene and Early Pleistocene (Fig. 9; Table 1).

Peak abundances of accessory species *Nonionella* spp. (*N. iridea, N. bradii*), and *Rosalina globularis* are most common during the MPT, particularly $\sim 15$–$12$ m b.s.f. ($\sim 1.20$–$0.96$ Ma; Fig. 9). *Nonionella* spp. and *R. globularis* also have a peak abundance at 33 m b.s.f. ($\sim 2.12$ Ma) and may be associated with MIS 81. Other typical Antarctic calcareous species, including *Astrononion* spp. (*A. echolsi, A. antarcticum*), *Ehrenbergina glabra*, *Alabaminella weddellensis*, and *Cibicides* spp. (*C. lobatulus, C. refulgens*), also show occasional peaks of abundance that likely correspond with interglacials and glacials of the Mid-Pleistocene Transition (MIS 37–MIS 31) and Late Pleistocene (MIS 15, MIS 11/10, MIS 7, MIS 6, and MIS 5). These taxa are all typically found in sub-ice-shelf environments of the Ross Sea continental shelf, particularly during deglacial and interglacial intervals (Osterman and Kellogg, 1979; Bernhard, 1987; Ward et al., 1987; Melis and Salvi, 2009; Bart et al., 2016; Capotondi et al., 2018; Majewski et al., 2018; Prothro et al., 2018; Majewski et al., 2020; Melis and Salvi, 2020; Melis et al., 2021). *Nonionella iridea* has been linked to elevated flux of phytodetritus (e.g., Gooday, 2003). *Nonionella* spp. are a secondary proxy of CDW incursion, sub-ice-shelf warming and basal melt, and a productivity proxy (Hillenbrand et al., 2017). Some small calcareous species, such as *Alabaminella weddellensis, Epistominella exigua*, and *Globocassidulina*

*subglobosa* rapidly colonize fresh phytodetritus, suggesting that these taxa may become dominant components of the fossil assemblages with episodic phytodetritus inputs (Jorissen et al., 2007). *Ehrenbergina glabra* has peak abundances in the same interval as *Globocassidulina biora* at 1.97–1.82 Ma (MIS 75–71). Assemblages with common *Cibicides lobatulus* or *C. refulgens* are useful proxies of strong currents and winnowed substrates since they live attached to invertebrates and coarser clasts, as does *Rosalina globularis* (Osterman and Kellogg, 1979; Bernhard, 1987; Mackensen et al., 1995; Gooday, 2003).

In summary, we interpret the *Globocassidulina* biofacies as times of a warmer Ross Sea with a weaker Antarctic Slope Current and incursions of CDW and mCDW. A major change in benthic foraminiferal biofacies occurs after ∼ 1.5 Ma, when *G. subglobosa* abundances fall off relative to *Trifarina earlandi*. A short-lived interval during the Mid-Pleistocene Transition (MIS 37-MIS 31) characterized by the *Trifarina-Rosalina-Nonionella* biofacies (green) may be associated with higher productivity along the shelf edge and incursions of CDW and mCDW during warmer interglacials. We interpret the increasing relative abundances of *Trifarina earlandi* as reflecting an increasing influence of the Antarctic Slope Current during the mid to Late Pleistocene (Table 1). Collectively, peaks of accessory calcareous benthic taxa may be indicative of CDW and mCDW impingement at shelf edge Site U1523 during the mid to Late Pleistocene (green biofacies; Figs. 6, 7) when the Antarctic Slope Current was less vigorous (e.g., Conte et al., 2021). At other times during the last 600 kyr, such as MIS 14, MIS 13, MIS 9, and Termination I or MIS 1, the Antarctic Slope Current was stronger and prevented incursion of CDW and mCDW as suggested by the dominance (> 65 %) of *Trifarina earlandi* (blue biofacies; Fig. 8, Table 1). The variable abundance to dominance of *T. earlandi* may prove to be a good proxy of Antarctic Slope Current strength and effectiveness as a barrier to the incursion of CDW and mCDW onto the Ross Sea continental shelf.

### 4.3 Possible Late Pliocene–Early Pleistocene warm intervals: 3.7 to 1.8 Ma

Planktic foraminiferal assemblages are dominated by *Neogloboquadrina pachyderma*, which is typical for the Ross Sea (Melis and Salvi, 2009). The planktic assemblages include rare *N. incompta* and very rare *Globigerina bulloides, G. falconensis*, and *Turborotalita quinqueloba* (Fig. 5). There are four periods with temperate water taxa present in the interval of ∼ 3.72–1.82 Ma, which could be evidence indicating incursions of warmer waters into the Ross Sea, affecting the ice cover and ice sheet stability. Temperate–subpolar *T. quinqueloba* peaks at ∼ 3.7–3.6 Ma. Temperate *Globoconella inflata* and tropical–subtropical *Globigerinoides ruber* are present in a single sample at ∼ 2.95 Ma in the uppermost Pliocene. Temperate *G. bulloides* has a small peak at ∼ 2.32 Ma, while temperate *G. falconensis* peaks from ∼ 1.97–1.82 Ma. These four peaks could represent incursions of warmer water reaching the Ross Sea during interglacials, which our age model place at MIS Gi7–Gi3 (∼ 3.72–3.65 Ma), MIS G17 (∼ 2.95 Ma), MIS 91 (∼ 2.32 Ma), and the interval MIS 77–67 (∼ 1.97–1.82 Ma) (Lisiecki and Raymo, 2005; Fig. 9; Table 1). These species were likely not living on the Ross Sea shelf, but instead were transported with warmer-water currents of the Ross Gyre, or perhaps by incursions of mCDW onto the shelf from the north that were able to break through a weakened Antarctic Slope Current during this time period. Temperate water planktic foraminiferal species are not recorded at Site U1523 after ∼ 1.82 Ma, signaling continued cooling and isolation of the Ross Sea from warmer surface waters swept in by the Ross Gyre and/or mCDW incursions. From the perspective of inter-hemispheric teleconnections, it is interesting to note that perennial lake ice cover at Lake El'gygytgyn in northeastern Russia does not appear until 1.8 Ma (Melles et al., 2012; Brigham-Grette et al., 2013).

Gales et al. (2023) identified weak layers (WL-2, WL-1, WL-1b), consisting of diatomite and diatom ooze or diatom-rich mud, beneath three submarine landslides on the upper slope of the Ross Sea, near the head of Hillary Canyon. The diatomaceous weak layers are interbedded with glaciomarine diamicts; two are Late Pliocene in age and one is Middle Miocene. The weak layers are recorded in IODP Site U1523, and correspond in part with the mid-Piacenzian Warm Period (mPWP, 3.264–3.025 Ma; Dowsett et al., 2011; Haywood et al. 2016) and the Miocene Climatic Optimum (MCO; Shevenell et al., 2004, 2008; Holbourn et al., 2022), respectively. The two Late Pliocene weak layers were deposited during times of open marine conditions and high biosiliceous productivity along the Ross Sea shelf edge. Here we slightly reinterpret the age of the upper weak layer 1b, which includes the presence of temperate water *Globoconella inflata* (6 specimens) and tropical-subtropical *Globigerinoides ruber* (4 specimens) in Sample U1523B-5F-3, 35–37 cm, as most likely correlative with MIS G17 (2.95 Ma; Liesiecki and Raymo, 2005), rather than the WL-1b interval spanning MIS G15 to MIS G11 (∼ 2.91–2.82 Ma) as published in Gales et al. (2023) (Fig. 9). This reinterpretation of weak layer 1b age is based on following evidence: (1) MIS G17 was a warm "super-interglacial" that is arguably a continuation of the mPWP (Raymo et al., 2011); (2) Taylor-Silva and Riesselman (2018) recognize multiple intervals of southward Polar Front migration during the mid to Late Pliocene of IODP Site U1361 off the Wilkes Land margin based on diatom preservation, absolute diatom abundance, and percentage of biogenic silica, including MIS G17; (3) a significant interval of ice retreat and diatomite deposition is recognized in the AND-1B core that is correlative with MIS G17 (Naish et al., 2009; McKay et al., 2012); (4) Dwyer and Chandler (2009) report a 25 m or higher highstand linked to MIS G17 based on coupled benthic Mg / Ca paleotempera-

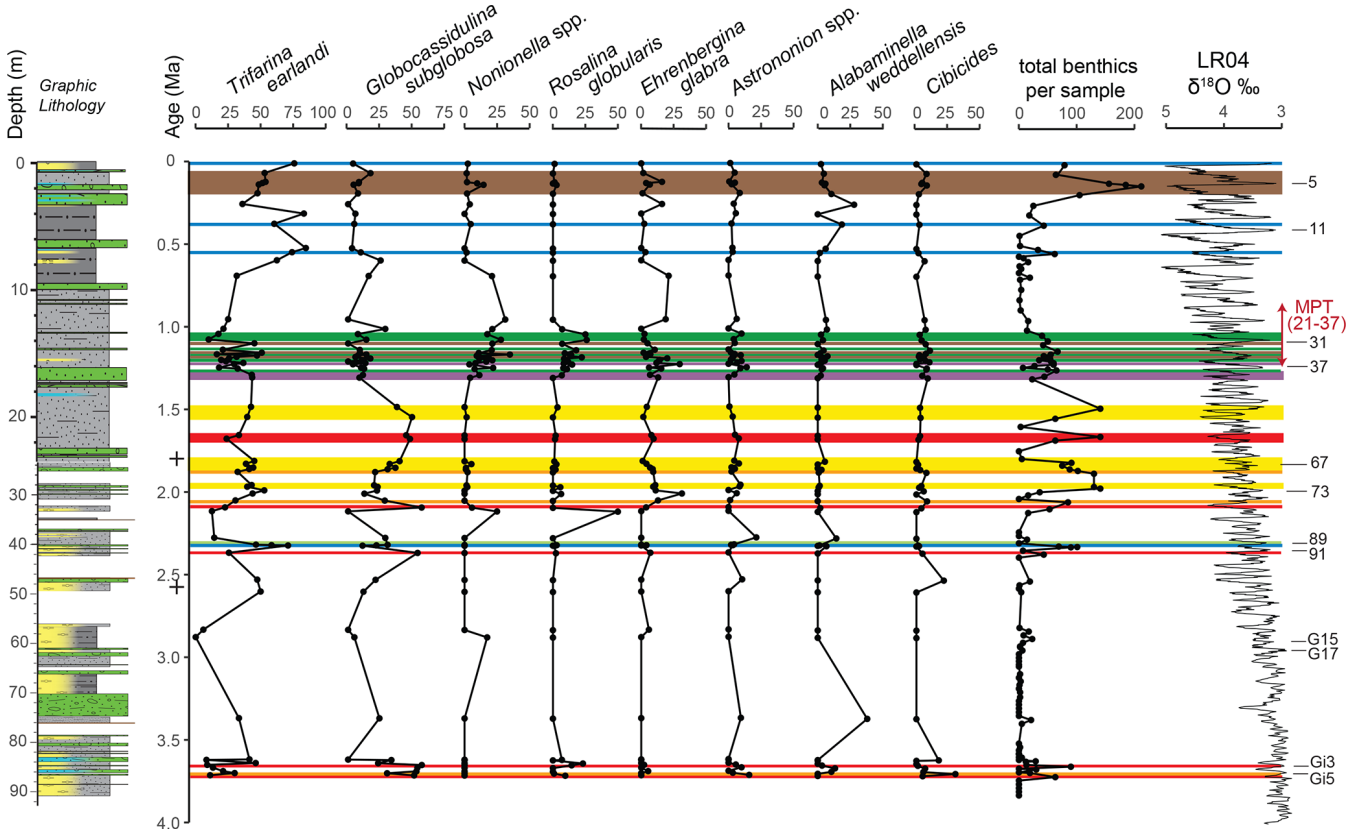


**Figure 8.** Benthic foraminiferal biofacies at Site U1523 based on Q-mode and R-mode cluster analysis and the Bray–Curtis similarity index. Only includes samples with 40 or more specimens ($N = 42$). Color-coded horizontal bars represent biofacies defined in Fig. 7. Note the major change in benthic foraminiferal biofacies after ~ 1.5 Ma: from *Globocassidulina subglobosa*-dominant or co-dominant biofacies (red, orange, yellow) to *Trifarina earlandi*-dominant biofacies (blue, brown, purple, green), reflecting the increasing influence of the Antarctic Slope Current in the mid to Late Pleistocene. The graphic lithology is from Gales et al. (2023). The two + symbols in the age column mark the position of the two magnetic reversals that help define the age model used for Site U1523.

tures and oxygen isotopes; and (5) Ishino and Suto (2020) provide diatom evidence for the expansion of sea ice south of the Kerguelen Plateau at ~ 2.9 Ma, which postdates the warmth of MIS G17. We suggest that the lower weak layer 1 (Gales et al., 2023) is correlative with MIS KM3 (~ 3.16 Ma; Liesiecki and Raymo, 2005) during the mPWP although our two foraminiferal samples from Section U1523B-7F-2 contain only rare planktics and no warm-water taxa (Fig. 9). There may have been warming and ice sheet instability around the time of the *G. ruber* and *G. inflata* occurrence at Site U1523 in the latest Pliocene. These warmer-water taxa were likely transported to the edge of the Ross Sea by the Ross Gyre (Dotto et al., 2018). Weak layer 1 overlies a coarse diamicton that is likely correlative with the MIS M2 glaciation (~ 3.3 Ma), a period of glacial expansion in the Ross Sea (McKay et al., 2012a, b).

Our findings from Site U1523 at the edge of the Ross Sea suggest multiple warm-water incursions during the Pliocene through Mid-Pleistocene. Sedimentological evidence from ice-proximal AND 1-B suggests that peak interglacials prior to 2.58 Ma had reduced sea-ice (Naish et al., 2009; McKay et al., 2012a). Sedimentological data and the number of planktic and benthic foraminifera per gram also provide supporting evidence for these likely warm periods. These time periods show increased numbers of planktics and benthics per gram of sediment compared to the background, which indicates higher productivity possibly from less ice cover, especially during MIS 77–67 (~ 2.03–1.83 Ma), which along with the interval of MIS 37–31 (~ 1.23–1.07 Ma) and MIS 5e (123 ka), have the highest foraminifera per gram of sediment. The temperate species often occur along with a decreased weight percent of fine sediment (silt and clay), which indicates more sand particles due to either ice rafting or strengthened bottom currents leading to winnowing of the fines and better preservation of carbonate.

### 4.4 MIS 31 and the MPT

The foraminifera per gram, especially planktic, and the number of benthic species are high through the MPT, while in the sediment data, the percent fine sediment decreases

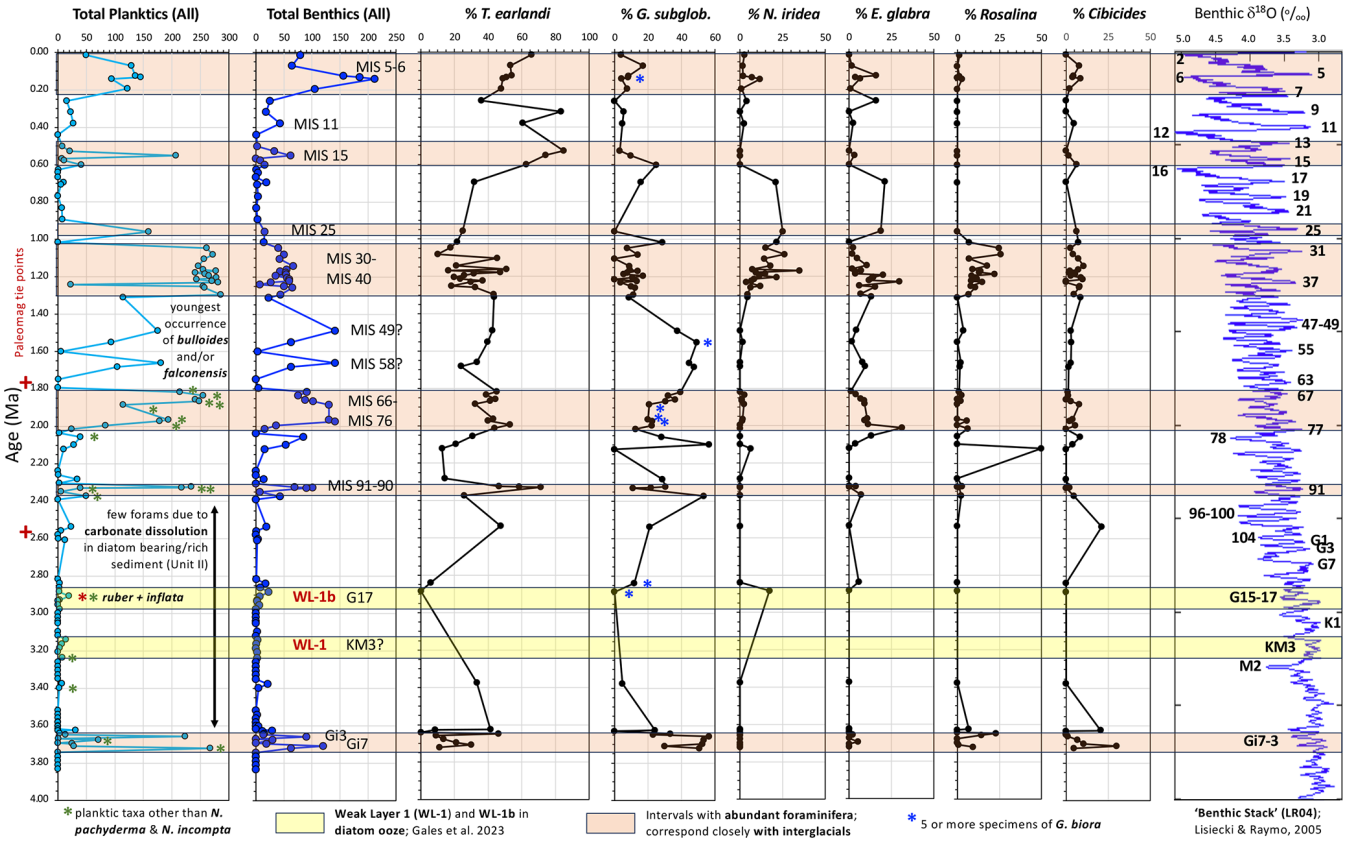


**Figure 9.** Summary of foraminiferal data from Site U1523, including the numbers of planktic and benthic specimens in all 131 samples investigated, and the percent of key benthic foraminifera based on all samples with at least 10 benthic specimens (66 samples; 50.4 %). Pink bars highlight intervals of the studied section with greater abundances of foraminifera. Carbonate dissolution in Unit II sediments is suspected to be the principal reason for barren samples or low foraminiferal abundances between ~ 3.6 and 2.4 Ma. The two yellow bars represent intervals of diatom ooze that were glide planes for submarine landslides above Hillary Canyon (weak layers WL-1b and WL-1; Gales et al., 2023). Weak layer WL-1b likely correlates with Marine Isotope Stage G17, a super-interglacial of the Latest Pliocene (see discussion in text). Note the last occurrence of warmer-water planktic foraminiferal taxa (green asterisk: *Globigerina bulloides, G. falconensis*, and *Turborotalita quinqueloba*) is ~ 1.82 Ma at Site U1523.

before, during and after MIS 31 (Fig. 4). A higher number of foraminifera could indicate that the time period of MIS 37–MIS 31 (~ 1.23–1.03 Ma), and including MIS 25 (~ 0.96 Ma), had in general higher productivity, particularly during the interglacials, interpreted to be created by reduced sea ice cover and/or retreat of the Ross Ice Shelf. Less fine-grained material indicates greater abundances of sand- and pebble-sized particles, due to increased melting and ice rafting, vigorous bottom currents causing winnowing, or reduced diatom productivity. MIS 31 may have been unusually warm and long in Antarctica leading to a collapse or partial collapse of the WAIS (Scherer et al., 2008; Naish et al., 2009; McKay et al., 2012b). Villa et al. (2010) report a low-abundance, low-diversity calcareous nannofossil assemblage in the MIS 31 interval of drill site AND-1B adjacent to the Transantarctic Mountains, which they attribute to warmer, ice-free conditions in the McMurdo Sound area and a weaker frontal system in the Southern Ocean. Studies around the Southern Ocean (Teitler et al., 2015), as well as in the Russian Arctic at Lake El'gygytgyn (de Wet et al., 2016; Lindberg et al., 2022), have found evidence for the time period surrounding MIS 31 to have included other unusually warm interglacials. We see evidence at Site U1523 of a longer interval of warming in this area of the Ross Sea, spanning MIS 37 to MIS 31 and extending to MIS 25, that was more productive, with reduced ice cover and greater flux of planktic foraminifera. However, no temperate planktic foraminiferal species were found during this time (Fig. 9).

An abrupt increase in planktic foraminiferal fragmentation ~ 900 ka signals a major change in oceanographic conditions along the shelf break at Site U1523. Elderfield et al. (2012) attribute the MIS 24–MIS 22 interval (the "900 ka event") to an abrupt increase in Antarctic ice volume. The increasing abundances of *Trifarina earlandi* at Site U1523 after ~ 1.5 Ma, and particularly after 600 ka, suggest greater current strength of the ASC.

### 4.5 MIS 15 and MIS 5e

Two additional times of increased foraminifers per gram of sediment and increased benthic species diversity generally correlate with Late Pleistocene MIS 15 (∼ 550 ka) and Termination II at the end of MIS 6 and MIS 5e (∼ 133–126 ka). A high number of planktic foraminifera in Antarctic waters could indicate higher productivity that possibly caused less sea ice cover or from the retreating ice shelf. Around MIS 5e is the highest planktics per gram of the entire record, which is a strong indicator for higher productivity during this interglacial. However, no temperate planktic species were found during these times. A decrease in the percent of fine-grained sediment by weight also occurs, which likely indicates increased winnowing from stronger currents as suggested by the dominance of the *Trifarina earlandi* biofacies (Figs. 7 and 8).

## 5 Conclusions

Repeated changes in planktic and benthic foraminiferal abundances, and in species relative abundances at IODP Site U1523, reflect the dynamic nature of water masses, circulation, productivity, and carbonate preservation during the Pliocene and Pleistocene (since 3.83 Ma) at Site U1523, with some of the most dramatic changes in benthic foraminiferal assemblages occurring during and after the Mid-Pleistocene Transition (MPT). A decrease in sedimentation rate from 3.352 to 1.219 cm $kyr^{-1}$ after 1.78 Ma suggests colder, drier conditions in the Ross Sea during the Mid- to Late Pleistocene (Naish et al., 2009; McKay et al., 2012a) and/or increased winnowing by currents along the edge of the continental shelf. The strength of the Antarctic Slope Current (ASC) and its influence on Circumpolar Deep Water (CDW) access to the Ross Sea continental shelf are suspected to be key drivers of the changing Pliocene–Pleistocene foraminiferal assemblages at IODP Site U1523.

The occurrence of rare temperate species of planktic foraminifera during the Pliocene and Early Pleistocene suggests an influx of CDW onto the Ross Sea shelf and periods of warmer-than-present conditions in the Ross Sea when there was more open water and less sea ice and a reduced to absent Ross Ice Shelf during interglacials (McKay et al., 2012b). Multiple incursions of rare warmer water taxa (*Globigerina bulloides*, *G. falconensis*, and *Turborotalita quinqueloba*) are associated with higher abundances of foraminifera (forams per gram of sediment). No temperate species occur at Site U1523 on the shelf break northeast of Pennell Bank after ∼ 1.82 Ma. Incursions of warm water taxa likely represent interglacials (Lisiecki and Raymo, 2005; MIS, Marine Isotope Stages) of the mid-Pliocene, including MIS Gi7-Gi5-Gi3 (∼ 3.72–3.65 Ma), Late Pliocene MIS G17 (∼ 2.95 Ma), and Early Pleistocene MIS 91 (∼ 2.32 Ma) and MIS 77-67 (∼ 2.0–1.83 Ma), indicating less ice cover in the Ross Sea and perhaps increased polar amplification during super-interglacials. Thin intervals of diatom ooze deposition in the uppermost Pliocene at Site U1523 correspond with Weak Layers 1 and 1b (submarine landslide glide planes; Gale et al., 2023), likely deposited during super interglacials MIS G17 (∼ 2.95 Ma), based on the presence of subtropical *Globigerinoides ruber* and temperate *Globoconella inflata* and MIS KM3 (∼ 3.16 Ma) during the mid-Piacenzian Warm Period (Dowsett et al., 2011; Raymo et al. 2011). Higher abundances of foraminifera in the Mid- to Late Pleistocene associated with MIS 37–31 (∼ 1.23–1.07 Ma), MIS 25 (∼ 0.96 Ma), MIS 15 (∼ 0.55 Ma), and Termination II–MIS 5e (∼ 0.133–0.126 Ma) may also indicate a reduced ice shelf and relatively warmer conditions. The abundance of foraminifera suggests multiple warmer interglacials during the MPT.

We hypothesize that the *Globocassidulina subglobosa* biofacies are associated with incursions of relatively warm, carbonate ($CO_3^{2-}$) and nutrient-rich Circumpolar Deep Water (CDW) or mCDW, and these incursions were more intense during interglacials of the Pliocene and Early Pleistocene when Antarctic Slope Current flow is suspected to have been generally weaker. The *Trifarina earlandi* biofacies are associated with stronger bottom-water currents along the shelf break due to higher ASC velocities during glacials and interglacials.

A major change in benthic foraminiferal biofacies occurred at Site U1523 prior to the Mid-Pleistocene Transition, ∼ 1.5 Ma. The increasing presence of *T. earlandi* during the Mid- to Late Pleistocene, especially during and after MIS 15 (∼ 600 ka), likely indicates intensified bottom-water currents, including the westward-flowing, wind-driven ASC. The observed decrease in sedimentation rates after 1.78 Ma may signal the increased strength of the ASC and winnowing of fine-grained sediments along the shelf break. Alternatively, a change in Antarctic climate from relatively warm and wet (i.e., greater turbidity from glacial meltwater) to colder and drier conditions may have been another contributing factor to lower-sedimentation rates. Benthic foraminiferal biofacies analysis suggests that the ASC was relatively strong during glacials of the Pliocene and Early Pleistocene but weaker during interglacials. However, after ∼ 1.82 Ma, the strong correlation of *Trifarina earlandi* abundance with both glacials and interglacials suggests that there has been a baseline increase in ASC strength since the latest Early Pleistocene.

In summary, we suggest that the Ross Sea became progressively isolated from the Southern Ocean by stronger flow of the Antarctic Circumpolar Current (ACC), Ross Gyre, and Antarctic Slope Current before and during the Mid-Pleistocene based on the last occurrence of temperate planktic foraminifera (∼ 1.82 Ma), a decrease in sedimentation rates due to cooling climate and/or increased current winnowing after 1.78 Ma, a major change in benthic foraminiferal biofacies (∼ 1.5 Ma), and an increase in foraminiferal fragmentation after the MPT (∼ 0.9 Ma).

The marked increase in foraminiferal fragments after the Mid-Pleistocene Transition suggests corrosive waters and/or stronger flow of the ASC along the shelf edge and water masses entering and exiting the Ross Sea.

Importantly, rare warmer water species of planktic foraminifera are recorded sporadically in Ross Sea cores from the Early Pleistocene back through the Early and Middle Miocene (e.g., Leckie and Webb, 1986; Bombard et al., 2024; this study), reflecting times when the Antarctic Polar Front was situated further south (closer to Antarctica), the strength of the temperature gradient across the Antarctic Polar Front was weaker, and/or strength of the Antarctic Circumpolar Current, Ross Gyre, and Antarctic Slope Current were weaker. These factors, alongside the reduced ice cover on the continental shelf, resulted in a fundamentally different oceanographic regime in the Ross Sea and would have likely significantly impacted the formation of Antarctic surface and bottom waters, which are critical for global heat transport and ecosystems in the Antarctic. The record of occasional warm water taxa provides evidence for polar amplification during some interglacials of the Pliocene and Early Pleistocene.

**Data availability.** Data are published on ScienceBase, the USGS data repository: https://www.sciencebase.gov/catalog/item/653914f0d34ee4b6e05bbb1e (Seidenstein and Mark Leckie, 2023).

**Sample availability.** Microfossil specimens from this study are stored at the University of Massachusetts Micropaleontology Lab.

**Team list.** IODP Expedition 374 Scientists: Jeanine Ash (Department of Earth, Environmental and Planetary Sciences, Rice University, Houston, USA), François Beny (Laboratoire d'Océanologie et de Géosciences, Université de Lille I, Villeneuve d'Ascq, France), Imogen M. Browne (College of Marine Science, University of South Florida, St. Petersburg, USA), Giuseppe Cortese (GNS Science, Lower Hutt, New Zealand), Laura De Santis (Instituto Nazionale di Oceanografia e di Geofisica Sperimentale (OGS), Trieste, Italy), Justin P. Dodd (Department of Earth, Atmosphere and Environmental Geosciences, Northern Illinois University, USA), Oliver M. Esper (Alfred Wegener Institute, Bremerhaven, Germany), Jenny A. Gales (School of Biological and Marine Sciences, University of Plymouth, Plymouth, UK), David M. Harwood (Earth and Atmospheric Sciences, University of Nebraska, Lincoln, USA), Saki Ishino (Department of Earth and Planetary Sciences, Nagoya University, Nagoya, Japan), Benjamin A. Keisling (Department of Earth, Geographic, and Climate Science, University of Massachusetts, Amherst, USA), Sookwan Kim (Ocean Climate Response and Ecosystem Research Department, Korea Institute of Ocean Science and Technology, Busan, Republic of Korea), Sunghan Kim (Division of Polar Paleoenvironment, Korea Polar Research Institute, Republic of Korea), Denise K. Kulhanek (Institute of Geosciences, Christian-Albrecht University of Kiel, Kiel, Germany; Department of Earth Sciences, Binghamton University, State University of New York, Binghamton, USA), Jan Sverre Laberg (Department of Geosciences, UIT – The Arctic University of Norway, Tromsø, Norway), R. Mark Leckie (Department of Earth, Geographic, and Climate Science, University of Massachusetts, Amherst, USA), Robert M. McKay (Antarctic Research Centre, Victoria University of Wellington, Wellington, New Zealand), Juliane Müller (Alfred Wegener Institute, Bremerhaven, Germany), Molly O. Patterson (Department of Earth Sciences, Binghamton University, State University of New York, Binghamton, USA), Brian W. Romans (Geosciences, Virginia Tech, Blacksburg, USA), Oscar E. Romero (MARUM, University of Bremen, Bremen, Germany), Francesca Sangiorgi (Earth Sciences, University of Utrecht, Utrecht, The Netherlands), Osamu Seki (Institute of Low Temperature Science, Hokkaido University, Sapporo Hokkaido, Japan), Amelia E. Shevenell (College of Marine Science, University of South Florida, St. Petersburg, USA), Shiv M. Singh (Polar Biology Lab, National Centre for Antarctic and Ocean Research (NCAOR), Goa, India), Isabela M. Cordeiro de Sousa (Instituto de Geociencias, Universidade de Brasília, Brasilia, Brazil), Saiko T. Sugisaki (Marine Geology Research Group, Geological Survey of Japan, Tsukuba Ibaraki, Japan), Tina van de Flierdt (Department of Earth Science and Engineering, Imperial College London, London, UK), Tim E. van Peer (National Oceanography Centre Southampton, University of Southampton, Southampton, UK), Whenshen Xiao (State Key Laboratory of Marine Geology, Tongji University, Shanghai, China), Zhifang Xiong (First Institute of Oceanography, State Oceanic Administration, Qingdao, China).

**Author contributions.** RML came up with the concept for this study and aided in collecting cores and analyzing some of the samples during IODP expedition 374. JLS did the lab work for this study and analyzed the data with help from RML. DH provided key information related to the age model. JLS prepared the first drafts of the manuscript, and RML wrote a revised version with contributions from all co-authors.

**Competing interests.** The contact author has declared that none of the authors has any competing interests.

**Disclaimer.** Publisher's note: Copernicus Publications remains neutral with regard to jurisdictional claims made in the text, published maps, institutional affiliations, or any other geographical representation in this paper. While Copernicus Publications makes every effort to include appropriate place names, the final responsibility lies with the authors.

**Special issue statement.** This article is part of the special issue "Advances in Antarctic chronology, paleoenvironment, and paleoclimate using microfossils: Results from recent coring campaigns". It is not associated with a conference.

**Acknowledgements.** We thank the scientists and crew of IODP Expedition 374 to the Ross Sea in 2018. This research used data and samples provided by the International Ocean Discovery Program (IODP), which is sponsored by the US National Science

Foundation (NSF) and participating countries. This paper evolved from a Master's thesis presented by Julia L. Seidenstein in May 2020 and supported with funding from the University of Massachusetts graduate program in Geology and the U.S. Science Support Program. Thanks to Mike Jercinovic for assistance with the UMass Department of Geosciences Electron Microprobe/SEM Facility for use of the Carl Zeiss EVO50 variable pressure scanning electron microscope to take images of microfossil specimens for the plates. We acknowledge the very helpful and constructive reviews of Anieke Brombacher, Scott Ishman, and an anonymous referee. Thank you to Isla S. Castañeda, Robert M. DeConto, Marci Robinson, and Harry Dowsett for helpful comments on earlier versions of the manuscript. Thanks to Anne Jennings for discussions about Arctic foraminifera preservation and to Ellen Thomas for guidance on the statistics of low specimen counts. A special thank you to Denise Kulhanek for handling this paper as special editor and to our UMass Micropaleo lab mates Samantha Bombard, Serena Dameron, and Erin Kim for their input, feedback, and support.

**Financial support.** This research has been supported by NSF OCE 14-50528 to RML (grant no. 19747558).

**Review statement.** This paper was edited by Denise K. Kulhanek and reviewed by Wojciech Majewski, Scott Ishman, and Anieke Brombacher.

## References

Anderson, J. B.: Ecology and distribution of foraminifera in the Weddell Sea of Antarctica, Micropaleontology, 21, 69–96, 1975.

Azetsu-Scott, K., Clarke, A., Falkner, K., Hamilton, J., Jones, E. P., Lee, C., Petrie, B,, Prinsenberg, S., Starr, M., and Yeats, P.: Calcium carbonate saturation states in the waters of the Canadian Arctic Archipelago and the Labrador Sea, J. Geophys. Res.-Ocean., 115, C11021, doi.org/10.1029/2009JC005917, 2010.

Bamber, J. L., Riva, R. E., Vermeersen, B. L., and LeBrocq, A. M.: Reassessment of the potential sea-level rise from a collapse of the West Antarctic Ice Sheet, Science, 324, 901–903, https://doi.org/10.1126/science.1169335, 2009.

Bart, P. J., Coquereau, L., Warny, S., and Majewski, W.: *In situ* foraminifera in grounding zone diamict: A working hypothesis, Antarct. Sci., 28, 313–321, https://doi.org/10.1017/S0954102016000055, 2016.

Beltran, C., Golledge, N. R., Ohneiser, C., Kowalewski, D. E., Sicre, M.-A., Hageman, K. J., Smith, R., Wilson, G. S., and Mainié, F.: Southern Ocean temperature records and ice-sheet models demonstrate rapid Antarctic ice sheet retreat under low atmospheric $CO_2$ during Marine Isotope Stage 31, Quaternary Sci. Rev., 228, 106069, https://doi.org/10.1016/j.quascirev.2019.106069, 2020.

Bernhard, J. M.: Foraminiferal biotopes in Explorers Cove, McMurdo Sound, Antarctica, J. Foramin. Res., 17, 286–297, 1987.

Bohaty, S. M. and Harwood, D. M.: Southern Ocean Pliocene paleotemperature variation from high-resolution silicoflagellate biostratigraphy, Mar. Micropaleontol., 33, 241–272, 1998.

Bollen, M., Riesselman, C. R., Ohneiser, C., Albot, O., McKay, R., Lee, M. K., Yoo, K.-C., Kim, S., Lee, J. I., and Levy, R.: Pleistocene oceanographic variability in the Ross Sea: A multiproxy approach to age model development and paleoenvironmental analyses, Glob. Planet. Change, 216, 103901, https://doi.org/10.1016/j.gloplacha.2022.103901, 2022.

Bombard, S., Leckie, R. M., and and IODP Exp. 374 Science Party: Pleistocene foraminifera of the Ross Sea continental slope and rise, IODP Exp. 374, FORAMS23, June 2023, Perugia Italy, 2023.

Bombard, S., Leckie, R. M., Browne, I., Shevenell, A., McKay, R., Harwood, D. M., and IODP Exp 374 Science Party: Miocene Climatic Optimum and Middle Miocene Climate Transition: A foraminiferal record from the central Ross Sea, Antarctica, J. Micropalaeontol., accepted, 2024.

Bostock, H. C., Barrows, T. T., Carter, L., Chase, Z., Cortese, G., Dunbar, G. B., Ellwood, M., Hayward, B., Howard, W., Neil, H. L., Noble, T. L., Mackintosh, A., Moss, P. T., Moy, A. D., Williams, M. J. M., and Armand, L. K.: A review of the Australian-New Zealand sector of the Southern Ocean over the last 30 ka (Aus-INTIMATE project), Quaternary Sci. Rev., 74, 35–57, https://doi.org/10.1016/j.quascirev.2012.07.018, 2013.

Brigham-Grette, J., Melles, M., Minyuk, P., Andreev, A., Tarasov, P., DeConto, R., Koenig, S., Nowaczyk, N., Wennrich, V., Rosén, P., Haltia, E., Cook, T., Gebhardt, C., Meyer-Jacob, C., Snyder, J., and Herzschuh, U.: Pliocene warmth, polar amplification, and stepped Pleistocene cooling recorded in NE Arctic Russia, Science, 340, 1421–1427, https://doi.org/10.1126/science.1233137, 2013.

Budillon, G., Castagno, P., Aliani, S., Spezie, G., and Padman, L.: Thermocline variability and Antarctic Bottom Water formation at the Ross Sea shelf break, Deep-Sea Res. Pt. I, 58, 1002–1018, https://doi.org/10.1016/j.dsr.2011.07.002, 2011.

Capotondi, L., Bergami, C., Giglio, F., Langone, L., and Ravaioli, M.: Benthic foraminifera distribution in the Ross Sea (Antarctica) and its relationship to oceanography, B. Soc. Paleontol. Ital., 57, 187–202, https://doi.org/10.4435/BSPI.2018.12, 2018.

Castagno, P., Falco, P., Dinniman, M. S., Spezie, G., and Budillon, G.: Temporal variability of the Circumpolar Deep Water inflow onto the Ross Sea continental shelf, J. Mar. Syst., 166, 37–49, https://doi.org/10.1016/j.jmarsys.2016.06.009, 2017.

Coccioni, R. and Galeotti, S.: Foraminiferal biostratigraphy and paleoecology of the CIROS-1 Core from McMurdo Sound (Ross Sea, Antarctica), Terra Antarct., 4, 103–117, 1997.

Colleoni, F., De Santis, L., Siddoway, C. S., Bergamasco, A., Golledge, N. R., Lohmann, G., Passchier, S. and Siegert, M. J.: Spatio-temporal variability of processes across Antarctic ice-bed – ocean interfaces, Nat. Commun., 9, 2289, https://doi.org/10.1038/s41467-018-04583-0, 2018.

Conte R., Rebesco, M., De Santis, L., Colleoni, F., Bensi, M., Bergamasco, A., Kovacevic, V., Gales, J., Zgur, F., Accettella, D., De Steur, L., Ursella, L., McKay, R., Kim, S., Lucchi, R. G., and the IODP Expedition 374 Scientists: Bottom current control on sediment deposition between the Iselin Bank and the Hillary Canyon (Antarctica) since the Late Miocene: An integrated seismic-oceanographic approach, Deep-Sea Res. PT. I, 176, 103606, https://doi.org/10.1016/j.dsr.2021.103606, 2021.

Corliss, B. H.: Taxonomy of Recent deep-sea benthonic foraminifera from the southeast Indian Ocean, Micropaleontology, 25, 1–19, 1979.

Corliss, B. H.: Distribution of Holocene deep-sea benthonic foraminifera in the southwest Indian Ocean, Deep-Sea Res. Pt. A, 30, 95–117, 1983.

DeConto, R. M., Pollard, D., and Kowalewski, D.: Modeling Antarctic ice sheet and climate variations during Marine Isotope Stage 31, Glob. Planet. Change, 96, 181–188, https://doi.org/10.1016/j.gloplacha.2012.05.018, 2012.

DeConto, R. M. and Pollard, D.: Contribution of Antarctica to past and future sea-level rise, Nature, 531, 591–597, https://doi.org/10.1038/nature17145, 2016.

de Wet, G. A., Castañeda, I. S., DeConto, R. M., and Brigham-Grette, J.: A high-resolution mid-Pleistocene temperature record from Arctic Lake El'gygytgyn: a 50 kyr super interglacial from MIS 33 to MIS 31?, Earth Planet. Sc. Lett., 436, 56–63, https://doi.org/10.1016/j.epsl.2015.12.021, 2016.

Diester-Haass, L., Billups, K., and Lear, C.; Productivity changes across the mid-Pleistocene climate transition, Earth-Sci. Rev., 179, 372–391, https://doi.org/10.1016/j.earscirev.2018.02.016, 2018.

Dinniman, M. S., Klinck, J. M., and Smith, Jr., W. O.: A model study of Circumpolar Deep Water on the West Antarctic Peninsula and Ross Sea continental shelves, Deep-Sea Res. Pt. II, 28, 1508–1523, https://doi.org/10.1016/j.dsr2.2010.11.013, 2011.

Dotto, T. S., Garabato, A. N., Bacon, S., Tsamados, M., Holland, P. R., Hooley, J., Frajka-Williams, E., Ridout, A., and Meredith, M. P.: Variability of the Ross Gyre, Southern Ocean: Drivers and responses revealed by satellite altimetry, Geophys. Res. Lett., 45, 6195–6204, https://doi.org/10.1029/2018GL078607, 2018.

Dowsett, H. J., Haywood, A. M., Valdes, P. J., Robinson, M. M., Lunt, D. J., Hill, D. J., Stoll, D. K., and Foley, K. M.: Sea surface temperatures of the mid-Piacenzian Warm Period: A comparison of PRISM3 and HadCM3, Palaeogeogr. Palaeocl., 309, 83–91, https://doi.org/10.1016/j.palaeo.2011.03.016, 2011.

Duplessy, J. C., Roche, D. M., and Kageyama, M.: The deep ocean during the last interglacial period, Science, 316, 89–91, https://doi.org/10.1126/science.1138582, 2007.

Dwyer, G. S. and Chandler, M. A.: Mid-Pliocene sea level and continental ice volume based on coupled benthic Mg/Ca palaeotemperatures and oxygen isotopes, Philos. T. R. Soc. A, 367, 157–168, 2009.

Elderfield, H., Ferretti, P., Greaves, M., Crowhurst, S., McCave, I. N., Hodell, D. A., and Piotrowski, A. M.: Evolution of ocean temperature and ice volume through the mid-Pleistocene climate transition, Science, 337, 704–709, https://doi.org/10.1126/science.1221294, 2012.

Emerson, S. and Bender, M.: Carbon fluxes at the sediment-water interface of the deep-sea: Calcium carbonate preservation, J. Mar. Res., 39, 139–162, 1981.

Fillon, R. H.: Late Cenozoic foraminiferal paleoecology of the Ross Sea, Antarctica, Micropaleontology, 20, 129–151, https://doi.org/10.2307/1485056, 1974.

Freeman, N. M., Lovenduski, N. S., and Gent, P. R.: Temporal variability in the Antarctic Polar Front (2002–2014), J. Geophys. Res.-Ocean., 121, 7263–7276, https://doi.org/10.1002/2016JC012145, 2016.

Gales, J. A., McKay, R. M., De Santis, L., Rebesco, M., Laberg, J. S., Shevenell, A. E., Harwood, D., Leckie, R. M., Kulhanek, D. K., King, M., Patterson, M., Lucchi, R. G., Kim, S., Kim, S., Dodd, J., Seidenstein, J., Prunella, C., Ferrante, G. M., and IODP Exp 374 Scientists: Climate-controlled submarine landslides on the Antarctic continental margin, Nat. Commun., 14, 2714, https://doi.org/10.1038/s41467-023-38240-y, 2023.

Gales J., Rebesco M., De Santis L., Bergamasco A., Colleoni F., Kim S., Accettella D., Kovacevic V., Liu Y., Olivo E., Colizza E., Florindo-Lopez C., Zgur F., and McKay R.: Role of dense shelf water in the development of Antarctic submarine canyon morphology, Geomorphology, 372, 107453, https://doi.org/10.1016/j.geomorph.2020.107453, 2021.

Gooday, A. J.: Benthic foraminifera (Protista) as tools in deep-water paleoceanography: Environmental influences on faunal characteristics, Adv. Mar. Biol., 46, 1–90, 2003.

Grant, G. R., Naish, T. R., Dunbar, G. B., Stocchi, P., Kominz, M. A., Kamp, P. J. J., Tapia, C. A., McKay, R. M., Levy, R. H., and Patterson, M. O.: The amplitude and origin of sea-level variability during the Pliocene epoch, Nature, 574, 237–241, https://doi.org/10.1038/s41586-019-1619-z, 2019.

Hammer, Ø., Harper, D. A. T., and P. D. Ryan, P. D.: PAST: Paleontological Statistics Software Package for Education and Data Analysis, Palaeontol. Electron., 4, 9 pp., http://palaeo-electronica.org/2001_1/past/issue1_01.htm (last access: 15 May 2024), 2001.

Hammer, Ø.: Reference Manual: PAST (PAleontological STatistics), version 4.13, Palaeontologia electronica, 2023.

Hauck, J., Gerdes, D., Hillenbrand, C.-D., Hoppema, M., Kuhn, G., Nehrke, G., Völker, C., and Wolf-Gladrow, D. A.: Distribution and mineralogy of carbonate sediments on Antarctic shelves, J. Mar. Syst., 90, 77–87, 2012.

Hauck, J., Arrigo, K. R., Hoppema, M., van Dijken, G. L., Völker, C., and Wolf-Gladrow, D. A.: Insignificant buffering capacity of Antarctic shelf carbonates, Global Biogeochem. Cy., 27, 1–10, https://doi.org/10.1029/2011GB004211, 2013

Hayward, B. W., Grenfell, H. R., Sabaa, A. T., and Neil H. L.: Factors influencing the distribution of Subantarctic deep-sea benthic foraminifera, Campbell and Bounty Plateaux, New Zealand, Mar. Micropaleontol., 62, 141–166, 2007.

Hearty, P. J., Hollin, J. T., Neumann, A. C., O'Leary, M. J., and McCulloch, M.: Global sea-level fluctuations during the Last Interglaciation (MIS 5e), Quaternary Sci. Rev., 26, 2090–2112, https://doi.org/10.1016/j.quascirev.2007.06.019, 2007.

Herbert, T. D.: The Mid-Pleistocene Climate Transition, Ann. Rev. Earth Planet. Sc., 51, 389–418, https://doi.org/10.1146/annurev-earth-032320-104209, 2023.

Hillenbrand, C.-D., Kuhn, G., and Frederichs, T.: Record of a Mid-Pleistocene depositional anomaly in West Antarctic continental margin sediments: An indicator for ice-sheet collapse?, Quaternary Sci. Rev., 28, 1147–1159, https://doi.org/10.1016/j.quascirev.2008.12.010, 2009.

Hillenbrand, C.-D., Smith, J. A., Hodell, D. A., Greaves, M., Poole, C. R., Kender, S., Williams, M., Andersen, T. J., Jernas, P. E., Elderfield, H., Klages, J. P., Roberts, S. J., Gohl, K., Larter, R. D., and Kuhn, G.: West Antarctic Ice Sheet retreat driven by Holocene warm water incursions, Nature, 547, 43–48, https://doi.org/10.1038/nature22995, 2017.

Hodell, D. A., Kennett, J. P., and Leonard, K. A.: Climatically induced changes in vertical water mass structure of the Vema Channel during the Pliocene: Evidence from DSDP Holes 516A, 517, and 518, in: Initial Reports of the Deep Sea Drilling Project, edited by: Barker, P. F., Carlson, R. L., and Johnson, D. A., National Science Foundation, 72, 907–919, 1983.

Holbourn, A., Kuhnt, W., Kochhann, K. G., Matsuzaki, K. M., and Andersen, N.: Middle Miocene climate–carbon cycle dynamics: Keys for understanding future trends on a warmer Earth?, https://doi.org/10.1130/2022.2556(05), 2022.

Ishino, S. and Suto, I.: Late Pliocene sea-ice expansion and its influence on diatom species turnover in the Southern Ocean, Mar. Micropaleontol., 160, 101895, https://doi.org/10.1016/j.marmicro.2020.101895, 2020.

Ishman, S. E. and Domack, E. W.: Oceanographic controls on benthic foraminifers from Bellingshausen margin of the Antarctic Peninsula, Mar. Micropaleontol., 24, 119–155, 1994.

Ishman, S. E. and Szymcek, P.: Foraminiferal distributions in the former Larsen-A Ice Shelf and Prince Gustav Channel region, eastern Antarctic Peninsula Margin: A baseline for Holocene paleoenvironmental change, in: Antarctic Peninsula Climate Variability: Historical and Paleoenvironmental Perspectives, edited by: Domack, E., Levente, A., Burnet, A., Bindschadler, R., Convey, P., and Kirby, M., 79, 239–260, https://doi.org/10.1029/AR079p0239, 2003.

Ishman, S. E. and Webb, P.-N.: Late Neogene benthic foraminifera from the Victoria Land Basin margin, Antarctica: Application to glacio-eustatic and tectonic events, Revue de paléobiologie, Special Volume 2, 523–551, 1988.

Jacobs, S. S.: On the nature and significance of the Antarctic Slope Front, Mar. Chem., 35, 9–24, 1991.

Jacobs, S. S., Bauer, E. B., Bruchhausen, P. M., Gordon, A. L., Root, T. F., and Rosselot, F. L.: Eltanin reports cruises 47–50 1971; 52–55 1972, hydrographic stations, bottom photographs, current measurements. nephelometer profiles, Tech. Rep. CU 2-74, LDGO, Columbia Univ., Palisades, NY, https://doi.org/10.7916/d8-3d9t-j927, 1974.

Jenkins, A., Dutrieux, P., Jacobs, S., Steig, E. J., Gudmundsson, G. H., Smith, J., and Heywood, K. J.: Decadal ocean forcing and Antarctic ice sheet response: Lessons from the Amundsen Sea, Oceanography, 29, 106–117, https://doi.org/10.5670/oceanog.2016.103, 2016.

Jorissen, F. J., Fontanier, C., and Thomas, E.: Paleoceanographical proxies based on deep-sea benthic foraminiferal assemblage characteristics, Dev. Mar. Geol., 1, 263–325, https://doi.org/10.1016/S1572-5480(07)01012-3, 2007.

Kellogg, T. B., Truesdale, R. S., and Osterman, L. E.: Late Quaternary extent of the West Antarctic ice sheet: new evidence from Ross Sea Cores, Geology, 7, 249–253, 1979.

Kennett, J. P.: Foraminiferal evidence of a shallow calcium carbonate solution boundary, Ross Sea, Antarctica, Science, 153, 191–193, https://doi.org/10.1126/science.153.3732.191, 1966.

Kennett, J. P.: The Fauna of the Ross Sea: Ecology and Distribution of Foraminifera, New Zealand Department of Scientific and Industrial Research, 186, 1–47, 1968.

Kim, S., Lee, J. I., McKay, R. M., Yoo, K.-C., Bak, Y.-S., Lee, M. K., Roh, Y. H., Yoon, H. I., Moon, H. S., and Hyun, C.-U.: Late Pleistocene paleoceanographic changes in the Ross Sea: Glacial-interglacieal variations in paleoproductivity, nutrient utilization, and deep-water formation, Quaternary Sci. Rev., 239, 106356, https://doi.org/10.1016/j.quascirev.2020.106356, 2020.

Kulhanek, D. K., Prunella, C., McLaughlin, J. R., Griffin, B., McKay, R. M., Patterson, M. O., Gales, J., Shevenell, A. E. and van Peer, T. E.: Data report: IODP Site U1523 composite section and stratigraphic splice based on X-ray fluorescence data, Proceedings of the International Ocean Discovery Program, 374.202, https://doi.org/10.14379/iodp.proc.374.202.2022, 2022.

Lagoe, M. B.; Recent benthonic foraminiferal biofacies in the Arctic Ocean, Micropaleontology, 25, 214–224, 1979.

Lamy, F., Winckler, G., Arz, H. W., Farmer, J. R., Gottschalk, J., Lembke-Jene, L., Middleton, J. L., van der Does, M., Tiedemann, R., Alvarez Zarikian, C., and Basak, C.: Five million years of Antarctic Circumpolar Current strength variability, Nature, 627, 789–796, https://doi.org/10.1038/s41586-024-07143-3, 2024.

Leckie, R. M. and Olson, H. C.: Foraminifera as proxies for sea-level change on siliciclastic margins, in: Micropaleontologic Proxies for Sea-Level Change and Stratigraphic Discontinuities, edited by: Olson, H. C. and Leckie, R. M., SEPM Society for Sedimentary Geology Special Publication No. 75, 5–19, https://doi.org/10.2110/pec.03.75.0005, 2003.

Leckie, R. M. and Webb, P.-N.: Late Oligocene-Early Miocene glacial record of the Ross Sea, Antarctica: Evidence from DSDP Site 270, Geology, 11, 578–582, 1983.

Leckie, R. M. and Webb, P.-N.: Late Paleogene and Early Neogene foraminifers of Deep Sea Drilling Project Site 270, Ross Sea, Initial Reports DSDP 90: 1093–1142, Washington, DC, US Government Printing Office, National Science Foundation, 1986.

Lindberg, K. R., Daniels, W. C., Castañeda, I. S., and Brigham-Grette, J.: Biomarker proxy records of Arctic climate change during the Mid-Pleistocene transition from Lake El'gygytgyn (Far East Russia), Clim. Past, 18, 559–577, https://doi.org/10.5194/cp-18-559-2022, 2022.

Lisiecki, L. E. and Raymo, M. E.: A Pliocene-Pleistocene stack of 57 globally distributed benthic $\delta^{18}$O records, Paleoceanography, 20, PA1003, https://doi.org/10.1029/2004PA001071, 2005.

Lythe, M. B., Vaughan, D. G., and Consortium: BEDMAP: A new ice thickness and subglacial topographic model of Antarctica, J. Geophys. Res.-Sol. Ea., 106, 11335–11351, https://doi.org/10.1029/2000JB900449, 2001.

Mackensen, A. and Berggren, W. A.: Paleogene benthic foraminifers from the southern Indian Ocean (Kerguelen Plateau): Biostratigraphy and paleoecology, edited by: Wise, S. W., Jr., Schlich, R., et al., in: Proceedings of the Ocean Drilling Program, 120, 603–630, 1992.

Mackensen, A., Schmiedl, G., Harloff, J., and Giese, M.: Deep-Sea foraminifera in the South Atlantic Ocean: Ecology and assemblage generation, Micropaleontology, 41, 342–358, 1995.

Majewski, W.: Benthic foraminiferal communities: Distribution and ecology in Admiralty Bay, King George Island, West Antarctica, Pol. Polar Res., 26, 159–214, 2005.

Majewski, W.: Benthic foraminifera from Pine Island and Ferrero bays, Admundsen Sea, Pol. Polar Res., 34, 169–200, https://doi.org/10.2478/popore-2013-0012, 2013.

Majewski, W., Wellner, J. S., and Anderson, J. B.: Environmental connotations for benthic foraminiferal assemblages from coastal West Antarctica, Mar. Micropaleontol., 124, 1–15, https://doi.org/10.1016/j.marmicro.2016.01.002, 2016.

Majewski, W., Bart, P. J., and McGlannan, A. J.: Foraminiferal assemblages from ice-proximal paleo-settings in the Whales Deep Basin, eastern Ross Sea, Antarctica, Palaeogeogr. Palaeocl., 493, 64–81, https://doi.org/10.1016/j.palaeo.2017.12.041, 2018.

Majewski, W., Prothro, L. O., Simkins, L. M., Demianiuk, E. J., and Anderson, J. B.: Foraminiferal patterns in deglacial sediment in the western Ross Sea, Antarctica: Life near grounding lines, Paleoceanography and Paleoclimatology, 35, 03716, https://doi.org/10.1029/2019PA003716, 2020.

Majewski, W., Holzmann, M., Gooday, A. J., Majda, A., Mamos, T., and Pawlowski, J.: Cenozoic climatic changes drive evolution and dispersal of coastal benthic foraminifera in the Southern Ocean, Sci. Rep., 11, 19869, https://doi.org/10.1038/s41598-021-99155-6, 2021.

Malinverno, E., Maffioli, P., and Gariboldi, K.: Latitudinal distribution of extant fossilizable phytoplankton in the Southern Ocean: Planktonic provinces, hydrographic fronts and palaeoeclogical perspectives, Mar. Micropaleontol., 123, 41–58, https://doi.org/10.1016/j.marmicro.2016.01.001, 2016.

McKay, R., Naish, T., Carter, L., Riesselman, C., Dunbar, R., Sjunneskog, C., Winter, D., Sangiorgi, F., Warren, C., Pagani, M. and Schouten, S.: Antarctic and Southern Ocean influences on Late Pliocene global cooling, P. Natl. Acad. Sci. USA, 109, 6423–6428, https://doi.org/10.1073/pnas.1112248109, 2012a.

McKay, R., Naish, T., Powell, R., Barrett, P., Scherer, R., Talarico, F., Kyle, P., Monien, D., Kuhn, G., Jackolski, C., and Williams, T.: Pleistocene variability of Antarctic Ice Sheet extent in the Ross Embayment, Quaternary Sci. Rev., 34, 93–112, https://doi.org/10.1016/j.quascirev.2011.12.012, 2012b.

McKay, R. M., De Santis, L., Kulhanek, D. K., and the Expedition 374 Scientists Ross Sea West Antarctic Ice Sheet History, Proceedings of the International Ocean Discovery Program, 374: College Station, TX (International Ocean Discovery Program), https://doi.org/10.14379/iodp.proc.374.2019, 2019.

McKnight Jr., W. M.: The distribution of foraminifera off parts of the Antarctic coast, Paleontological Research Institution, 44, 60–158, 1962.

Melis, R. and Salvi, G.: Late Quaternary foraminiferal assemblages from western Ross Sea (Antarctica) in relation to the main glacial and marine lithofacies, Mar. Micropaleontol., 70, 39–53, https://doi.org/10.1016/j.marmicro.2008.10.003, 2009.

Melis, R. and Salvi, G.: Foraminifer and ostracod occurrence in a cool-water carbonate factory of the Cape Adare (Ross Sea, Antarctica): A key lecture for the climatic and oceanographic variations in the last 30,000 years, Geosciences, 10, 413, https://doi.org/10.3390/geosciences10100413, 2020.

Melis, R., Capotondi, L., Torricella, F., Ferretti, P., Geniram, A., Hong, J. K., Kuhn, G., Khim, B.-K., Kim, S., Malinverno, E., Yoo, K. C., and Colizza, E.: Last Glacial Maximum to Holocene paleoceanography of the northwestern Ross Sea inferred from sediment core geochemistry and micropaleontology at Hallett Ridge, J. Micropalaeontol., 40, 15–35, https://doi.org/10.5194/jm-40-15-2021, 2021.

Melles, M., Brigham-Grette, J., Minyuk, P. S., Nowaczyk, N. R., Wennrich, V., DeConto, R. M., Anderson, P. M., Andreev, A. A., Coletti, A., Cook, T. L., and Haltia-Hovi, E.: 2.8 million years of Arctic climate change from Lake El'gygytgyn, NE Russia, Science, 337, 315–320, https://doi.org/10.1126/science.1222135, 2012.

Milam, R. W. and Anderson, J. B.: Distribution and ecology of recent benthonic foraminifera of the Adelie-George V continental shelf and slope, Antarctica, Mar. Micropaleontol., 6, 297–325, 1981.

Miller, K. G., Wright, J. D., Browning, J. V., Kulpecz, A., Kominz, M., Naish, T. R., and Sosdian, S.: High tide of the warm Pliocene: Implications of global sea level for Antarctic deglaciation, Geology, 40, 407–410, https://doi.org/10.1130/G32869.1, 2012.

Morard, R., Quillévéré, F., Douady, C. J., de Vargas, C., de Garidel-Thoron, T., and Escarguel, G.: Worldwide genotyping in the planktonic foraminifera *Globoconella inflata*: Implications for life history and paleoceanography, PLoS ONE, 6, e26665, https://doi.org/10.1371/journal.pone.0026665, 2011.

Morrison, A. K., Hogg, A. McC., England, M. H., and Spence, P.: Warm Circumpolar Deep-Water transport toward Antarctica driven by local dense water export in canyons, Sci. Adv., 6, eaav2516, https://doi.org/10.1126/sciadv.aav2516, 2020.

Naish, T., Powell, R., Levy, R., Wilson, G., Scherer, R., Talarico, F., Krissek, L., Niessen, F., Pompilio, M., Wilson, T., Carter, L., DeConto, R., Huybers, P., McKay, R., Pollard, D., Ross, J., Winter, D., Barrett, P., Browne, G., Cody, R., Cowan, E., Crampton, J., Dunbar, G., Dunbar, N., Florindo, F., Gebhardt, C., Graham, I., Hannah, M., Hansaraj, D., Harwood, D., Helling, D., Henrys, S., Hinnov, L., Kuhn, G., Kyle, P., Läufer, A., Maffioli, P., Magens, D., Mandernack, K., McIntosh, W., Millan, C., Morin, R., Ohneiser, C., Paulsen, T., Persico, D., Raine, I., Reed, J., Riesselman, C., Sagnotti, L., Schmitt, D., Sjunneskog, C., Strong, P., Taviani, M., Vogel, S., Wilch, T., and Williams, T.: Obliquity-paced Pliocene West Antarctic Ice Sheet oscillations, Nature, 458, 7236, https://doi.org/10.1038/nature07867, 2009.

Nakayama, Y., Menemenlis, D., Zhang, H., Schodlok, M., and Rignot, E.: Origin of Circumpolar Deep Water intruding onto the Amundsen and Bellingshausen Sea continental shelves, Nat. Commun., 9, 3403, https://doi.org/10.1038/s41467-018-05813-1, 2018.

Nelson, C. S. and Cooke, P. J.: History of oceanic front development in the New Zealand sector of the Southern Ocean during the Cenozoic – a synthesis, New Zeal. J. Geol. Geop., 44, 535–553, 2001.

Orsi, A. H. and Wiederwohl, C. L.: A recount of Ross Sea waters, Deep-Sea Res. Pt. II, 56, 778–795, https://doi.org/10.1016/j.dsr2.2008.10.033, 2009.

Osterman, L. E. and Kellogg, T. B.: Recent benthic foraminiferal distributions from the Ross Sea, Antarctica; relation to ecologic and oceanographic conditions, J. Foramin. Res., 9, 250–269, https://doi.org/10.2113/gsjfr.9.3.250, 1979.

Overpeck, J. T., Otto-Bliesner, B. L., Miller, G. H., Muhs, D. R., Alley, R. B., and Kiehl, J. T.: Paleoclimatic evidence for future ice-sheet instability and rapid sea-level rise, Science, 311, 1747–1750, https://doi.org/10.1126/science.1115159 2006.

Pagani, M., Liu, Z., LaRiviere, J., and Ravelo, A. C.: High Earth-system climate sensitivity determined from Pliocene carbon dioxide concentrations, Nat. Geosci., 3, 27–30, https://doi.org/10.1038/ngeo724, 2010.

Pardo, P. C., Pérez, F. F., Velo, A., and Gilcoto, M.: Water mass distribution in the Southern Ocean: Improvement of an extended OMP (eOMP) analysis, Prog. Oceanogr., 103, 92–105, https://doi.org/10.1016/j.pocean.2012.06.002, 2012.

Patterson, M. O. and Ishman, S. E.: Neogene benthic foraminiferal assemblages and paleoenvironmental record for McMurdo Sound, Antarctica, Geosphere, 8, 1331–1341, https://doi.org/10.1130/GES00771.1, 2012.

Patterson, M. O., McKay, R., Naish, T., Escutia, C., Jimenez-Espejo, F. J., Raymo, M. E., Meyers, S. R., Tauxe, L., Brinkhuis, H., and Expedition 318 Scientists: Orbital forcing of the East Antarctic ice sheet during the Pliocene and Early Pleistocene, Nat. Geosci., 7, 841–847, https://doi.org/10.1038/ngeo2273, 2014.

Peterson, L. C.: Recent abyssal benthic foraminiferal biofacies of the eastern equatorial Indian Ocean, Mar. Micropaleontol., 8, 479–519, 1984.

Peterson, L. C. and Lohmann, G. P.: Major change in Atlantic deep and bottom waters 700,000 yr ago: Benthonic foraminiferal evidence from the South Atlantic, Quaternary Res., 17, 26–38, 1982.

Pflum, C. E.: The distribution of foraminifera in the eastern Ross Sea, Amundsen Sea and Bellingshausen Sea, Antarctica, Paleontological Research Institution, 50, 151–209, 1966.

Pollard, D. and DeConto, R. M.: Modelling West Antarctic ice sheet growth and collapse through the past five million years, Nature, 458, 329–332, https://doi.org/10.1038/nature07809, 2009.

Pritchard, H., Ligtenberg, S. R. M., Fricker, H. A., Vaughan, D. G., Van den Broeke, M. R., and Padman, L.: Antarctic ice-sheet loss driven by basal melting of ice shelves, Nature, 484, 7395, https://doi.org/10.1038/nature10968, 2012.

Prothro, L. O., Simkins, L. M., Majewski, W., and Anderson, J. B.: Glacial retreat patterns and processes determined from integrated sedimentology and geomorphology records, Mar. Geol., 395, 104–119, https://doi.org/10.1016/j.margeo.2017.09.012, 2018.

Raymo, M. E., Mitrovica, J. X., O'Leary, J., DeConto, R. M., and Hearty, P. J.: Departures from eustasy in Pliocene sea-level records, Nat. Geosci., 4, 328–332, https://doi.org/10.1038/NGEO1118, 17 April 2011.

Sachs, O., Sauter, E. J., Schlüter, M., Rutgers van der Loeff, M. M., Jerosch, K., and Holby, O.: Benthic organic carbon flux and oxygen penetration reflect different plankton provinces in the Southern Ocean, Deep-Sea Res. Pt. I, 56, 1319–1335, https://doi.org/10.1016/j.dsr.2009.02.003, 2009.

Sanders, H. L.: Marine benthic diversity: A comparative study, Am. Nat., 102, 243–282, 1968.

Sangiorgi, F., Bijl, P. K., Passchier, S., Salzmann, U., Schouten, S., McKay, R., Cody, R. D., Pross, J., Van De Flierdt, T., Bohaty, S. M., Levy, R., Williams, T., Escutia, C. and Brinkhuis, H.: Southern Ocean warming and Wilkes Land ice sheet retreat during the mid-Miocene, Nat. Commun., 9, 1–11, https://doi.org/10.1038/s41467-017-02609-7, 2018.

Scherer, R. P., Aldahan, A., Tulaczyk, S., Possnert, G., Engelhardt, H., and Kamb, B.: Pleistocene collapse of the West Antarctic Ice Sheet, Science, 281, 82–85, https://doi.org/10.1126/science.281.5373.82, 1998.

Scherer, R. P., Bohaty, S. M., Dunbar, R. B., Esper, O., Flores, J. A., Gersonde, R., Harwood, D. M., Roberts, A. P., and Taviani, M.: Antarctic records of precession-paced insolation-driven warming during Early Pleistocene Marine Isotope Stage 31, Geophys. Res. Lett., 35, L03505, https://doi.org/10.1029/2007GL032254, 2008.

Schmiedl, G. and Mackensen, A.: Late Quaternary paleoproductivity and deep-water circulation in the eastern South Atlantic Ocean: Evidence from benthic foraminifera, Palaeogeogr. Palaeocl., 130, 43–80, 1997.

Seidenstein, J. L. and Leckie, R. M.: Pliocene-Pleistocene Warm Water Incursions and Water Mass Changes on the Ross Sea Continental Shelf (Antarctica) Based on Foraminifera, IODP Exp 374, USGS Data Release Products [data set], https://www.sciencebase.gov/catalog/item/653914f0d34ee4b6e05bbb1e (last access: 28 June 2024), 2023.

Shevenell, A. E., Kennett, J. P., and Lea, D. W.: Middle Miocene Southern Ocean cooling and Antarctic cryosphere expansion, Science, 305, 1766–1770, 2004.

Shevenell, A. E., Kennett, J. P., and Lea, D. W.: Middle Miocene ice sheet dynamics, deep-sea temperatures, and carbon cycling: A Southern Ocean perspective, Geochem. Geophy. Geosy., 9, Q02006, https://doi.org/10.1029/2007GC001736, 2008.

Si, Y. Stewart, A. L., and Eisenman, I.: Heat transport across the Antarctic Slope Front controlled by cross-slope salinity gradients, Sci. Adv., 9, eadd7049, https://doi.org/10.1126/sciadv.add7049, 2023.

Smith, W. O. Jr., Sedwick, P. N., Arrigo, K. R., Ainley, D. G., and Orsi, A. H.: The Ross Sea in a sea of change, Oceanography, 25, 90–103, https://doi.org/10.5670/oceanog.2012.80, 2012.

Smith, J. A., Graham, A. G. C., Post, A. L., Hillenbrand, C.-D., Bart, P. J., and Powell, R. D.: The marine geological imprint of Antarctic ice shelves, Nat. Commun., 10, 5635, https://doi.org/10.1038/s41467-019-13496-5, 2019.

Sokolov, S. and Rintoul, S. R.: Circumpolar structure and distribution of the Antarctic Circumpolar Current fronts: 1. Mean circumpolar paths, J. Geophys. Res.-Ocean., 114, C11018, https://doi.org/10.1029/2008JC005108, 2009.

Strong, C. P. and Webb, P.-N.: Oligocene and Miocene foraminifera from CRP-2/2A, Victoria Land Basin, Antarctica, Terra Antarct., 8, 461–472, 2000.

Strong, C. P. and Webb, P.-N.: Lower Oligocene foraminiferal fauna from CRP-3 Drillhole, Victoria Land Basin, Antarctica, Terra Antarct., 8, 347–358, 2001.

Szymcek, P., Ishman, S. E., Domack, E. W., and Leventer, A.: Holocene Oceanographic and Climatic Variability of the Vega Drift Revealed Through Foraminiferal Interpretation, Online Proceedings of the 10th ISAEC, edited by: Cooper, A. K. and Raymond, C. R., USGS Open-File Report, 1047, 2007.

Tagliaro, G., Fulthorpe, C. S., Watkins, D. K., De Vleeschouwer, D., Brumsack, H., Bogus, K., and Lavier, L. L.: Late Miocene-Pliocene vigorous deep-sea circulation in the Southeast Indian Ocean: Paleoceanographic and tectonic implications, Paleoceanogr. Paleocl., 37, e2021PA004303, https://doi.org/10.1029/2021PA004303, 2022.

Taylor-Silva, B. I. and Riesselman, C. R.: Polar frontal migration in the warm Late Pliocene: Diatom evidence from the Wilkes Land margin, East Antarctica, Paleoceanogr. Paleocl., 33, 76–92, doi.org/10.1002/2017PA003225, 2018.

Teitler, L., Florindo, F., Warnke, D. A., Filippelli, G. M., Kupp, G., and Taylor, B.: Antarctic Ice Sheet response to a long warm interval across Marine Isotope Stage 31: A cross-latitudinal study of iceberg-rafted debris, Earth Planet. Sc. Lett., 409, 109–119, https://doi.org/10.1016/j.epsl.2014.10.037, 2015.

Thompson, A. F., Stewart, A. L., Spence, P., and Heywood, K. J.: The Antarctic Slope Current in a changing climate, Rev.

Geophys., 56, 741–770, https://doi.org/10.1029/2018RG000624, 2018.

Villa, G., Persico, D., Wise, S., and Gadaleta, A.: Calcareous nannofossil evidence for Marine Isotope Stage 31 (1 Ma) in Core AND-1B, ANDRILL McMurdo Ice Shelf Project (Antarctica), Glob. Planet. Change, 96/97, 75–86, https://doi.org/10.1016/j.gloplacha.2009.12.003, 2010.

Wang, Y. Zhou, M., Zhang, Z., and Dinniman, M. S.: Seasonal variations in Circumpolar Deep Water intrusions into the Ross Sea continental shelf, Front. Mar. Sci., 10, 1020791, https://doi.org/10.3389/fmars.2023.1020791, 2023.

Ward, B. L. and Webb, P.-N.: Late Quaternary foraminifera from raised deposits of the Cape Royds-Cape Barne area, Ross Island, Antarctica, J. Foramin. Res., 16, 176–200, https://doi.org/10.2113/gsjfr.16.3.176, 1986.

Ward, B. L., Barrett, P. J., and Vella, P.: Distribution and ecology of benthic foraminifera in McMurdo Sound, Antarctica, Palaeogeogr. Palaeocl., 58, 139–153, https://doi.org/10.1016/0031-0182(87)90057-5, 1987.

Webb P.-N.: Benthic foraminifera, in: Antarctic Cenozoic history from the CIROS-1 Drillhole, edited by: Barrett, P. J., McMurdo Sound, DSIR Bull., 245, 99–118, 1989.

Webb, P.-N. and Strong, C. P.: Pliocene benthic foraminifera from CRP-2 (lithostratigraphic unit 2.2), Victoria Land Basin, Antarctica, Terra Antart., 7, 453–459, 2000.

Webb, P.-N. and Strong, C. P.: Foraminiferal biostratigraphy and palaecology in Upper Oligocene-Lower Miocene glacial marine sequences 9, 10, and 11, CRP-2/2A drill hole, Victoria Land Basin, Antarctica, Palaeogeogr. Palaeocl., 231, 71–100, https://doi.org/10.1016/j.palaeo.2005.07.036, 2006.

Webb, P.-N., Leckie, R. M., and Ward, B. L.: Foraminifera (Late Oligocene), in Barrett P.J. (ed.), Antarctic Cenozoic history from the MSSTS-1 Drillhole, McMurdo Sound, DSIR Bull., 237, 115–125, 1986.

Whitehead, J. M. and Bohaty, S.M.: Pliocene summer sea surface temperature reconstruction using silicoflagellates from Southern Ocean ODP Site 1165, Paleoceanography, 18, 1075, https://doi.org/10.1029/2002PA000829, 2003.

Whitworth III, T. and Orsi, A. H.: Antarctic Bottom Water production and export by tides in the Ross Sea, Geophys. Res. Lett., 33, L12609, https://doi.org/10.1029/2006GL026357, 2006.

Wilson, D. J., Bertram, R. A., Needham, E. F., Flierdt, T. van de, Welsh, K. J., McKay, R. M., Mazumder, A., Riesselman, C. R., Jimenez-Espejo, F. J., and Escutia, C.: Ice loss from the East Antarctic Ice Sheet during Late Pleistocene interglacials, Nature, 561, 383–386, https://doi.org/10.1038/s41586-018-0501-8, 2018.

Wu, S. Lembke-Jene, L., Lamy, F., Arz, H. W., Nowaczyk, N., Xiao, W., Zhang, Xu, Hass, H. C., Titschack, J., Zheng, X., Liu, J., Dumm, L., Diekmann, B., Nürnberg, D., Tiedemann, R., and Kuhn, G.: Orbital- and millennial-scale Antarctic Circumpolar variability in the Drake Passage over the past 140,000 years, Nat. Commun., 12, 3948, https://doi.org/10.1038/s41467-021-24264-9, 2021.